Impact of the SST and topography on the development of a large-hail storm event, on the Adriatic Sea

Antonio Ricchi [a,b,*], Lorenzo Sangelantoni [b,f], Gianluca Redaelli [a,b], Vincenzo Mazzarella [b], Mario Montopoli [c], Mario Marcello Miglietta [c], Alessandro Tiesi [c], Simone Mazzà [d], Richard Rotunno [e], Rossella Ferretti [a,b]

[a] University of L'Aquila, Department of Physics and Chemical Sciences, L'Aquila, Italy
[b] CETEMPS (Center of Excellence in Telesensing of Environment and Model Prediction of Severe Events), Italy
[c] CNR ISAC, Italy
[d] Università della Calabria, Italy
[e] NCAR, United States of America
[f] Climate Simulations and Predictions Division, Euro-Mediterranean Center on Climate Change (CMCC), Bologna, Italy

ABSTRACT

On July 10, 2019 an unusual and severe weather event hit Italy: a trough extending southward from northern Europe affected Italy and the Balkans, as it advected cold air over the Adriatic Sea, causing heavy damage because of giant hailstones reaching the ground. Between 08 UTC and 12 UTC of July 10, 2019, a deep convective cell developed along the coast of Marche in the vicinity of Ancona and quickly moved southward along the coast producing intense rainfall and hail, in particular near Pescara. In this work, the dynamics and thermodynamics responsible for triggering and maintaining the storm are investigated using the WRF (Weather Research and Forecasting) numerical model with the HAILCAST module activated. Several numerical experiments are carried out using a 1-km grid spacing with the aim of investigating in particular the impact of the orography and the SST anomaly in triggering and guiding the convective system. The results show that both the topography and the air-sea interaction played a key role: the topography guided the cold and dry air coming from the north, while the warm SST favored the instability of the environment. The SST anomaly plays a crucial role in creating the conditions necessary to generate the favorable conditions that led to the supercell and the giant hailstorm.

1. Introduction

In the Mediterranean area, Heavy Precipitation Events (HPEs) are generally driven by intense convective cells generated and sustained by the interaction of air masses with the orography and the Sea Surface Temperature (SST) (Nuissier et al., 2008Nuissier et al., 2011; Miglietta and Davolio, 2022). These events can be particularly destructive with strong socio-economic impacts.

Understanding and forecasting HPEs is still particularly challenging, especially if events are strongly localized. Several campaigns have been held in the Mediterranean basin (Khodayar et al., 2021) with the aim of highlighting both the triggering mechanisms and the physical processes producing heavy precipitation events, such as ALPEX in 1982 (Smith, 1982; Davies and Pichler, 1990), MAP in 1999 (Richard et al., 2007) and

HyMeX in 2012 (Ducrocq et al., 2014). As summarized in Khodayar et al., 2021 (HyMex campaign) the main mechanisms of heavy precipitation events (HPEs) over the western Mediterranean basin and its coastal areas are both large-scale forcings, such as baroclinic waves, Atlantic cyclone cut-offs, atmospheric rivers and air-sea ainteraction and local-scale factors such as convergence-line formation and interaction with the orography. Duffourg et al., 2016 highlighted how cyclonic circulations moving from the Atlantic, toward the Gulf of Lion, are responsible for low-level convergence over the Balearic Sea, causing HPEs events. Similarly, Barthlott and Davolio, 2016 showed how the formation of convergence lines behind Sardinia and Corsica, over the central and southern Tyrrhenian Sea, is a crucial factor for the formation of convective phenomena. This is due to the interaction of synoptic factors, such as the movement of baroclinic waves from the Atlantic

---

toward the Gulf of Lion and Gulf of Genoa, and local factors, such as the impact of the orography of the two islands. Lee et al., 2017 investigates the dynamics of HPEs over the Ebro basin, highlighting the crucial role of channelized flow in the Ebro valley. Wind-barrier and orography blocking are triggers for the development of intense HPEs in both southern France and the Po Valley, as shown in numerous studies in HyMex SOP and HyMex IOP2b and IOP6 and IOP18 (Pichelli et al., 2017; Davolio et al., 2015a; Miglietta et al., 2016a).

Generally, these campaigns took place during the autumn season because of the higher frequency of occurrence of severe events; their investigation allowed new insights into several mechanisms responsible for heavy rain, such as: local convergence, the role of orography and deep cyclogenesis (Rotunno and Ferretti, 2001; Rotunno and Houze, 2007; Ducrocq et al., 2014). The summer season shows a relatively low frequency of severe events and did not receive the same attention and thorough investigation.

However, the advection of continental cold air (Lionello et al., 2012) may occur even during summer and favor the development of convection over the warm Mediterranean Sea. These events are substantially modulated by the position of the Azores high pressure and of the subtropical northern African anticyclone, which may drive cold air masses toward the Mediterranean when they elongate at higher latitudes over the European regions; also, cyclogenesis may favor the cold air outbreaks from the Gulf of Lion or the Dinaric Alps (Blumen, 1992).

Depending on the formation mechanisms, the thunderstorms can be classified mainly as frontal and non-frontal. During late spring and summer, non-frontal thunderstorms are more frequent in Italy (Giaiotti et al., 2003): they develop along the mountain slopes, the Alps, and the Apennines, and are modulated by the strong radiation during the central hours of the day; then, they occasionally move toward the plains and the coastal areas (e.g., Manzato et al., 2014).

In many circumstances convection can be very intense, sometimes associated with supercells responsible for hail, tornadoes, and waterspouts (Avolio and Miglietta, 2023; Miglietta and Matsangouras, 2018; Miglietta et al., 2017b; Antonescu et al., 2017). Supercells occur frequently both on the plains of northern Italy and along the northern Adriatic coast where the moist and warm atmospheric flow from the Adriatic Sea interacts with the cooler air deflected by the orography enhancing upward motion at the border of the two air masses (Davolio et al., 2015b; Punge et al., 2017; Bagaglini et al., 2021). In the past, some supercells have been analyzed in northeastern Italy using both observations (Manzato et al., 2014; Pucillo et al., 2020) and numerical simulations (Miglietta et al., 2016b), showing a limited predictability and a strong sensitivity to the initial conditions. At least for tornado-spawning supercells, positive Sea Surface Temperature (SST) anomalies are found before their development (Bagaglini et al., 2021). Previous studies have focused on the formation of HPEs in central and southern Italy, in particular Silvestri et al., 2022 described the connection between circulation, orography and HPEs over central Italy. Capozzi et al., 2023 investigates precipitation types and patterns that may impact the Campania region (southern Italy), as does Miglietta and Regano, 2008 for a HPE event over Apulia (Southeastern Italy) and Mastrangelo et al., 2011 for the HPE event that occurred in 2004 between Apulia and Basilicata. In addition, Mazzarella et al., 2020 is relevant for the area under investigation, studying the application of radar, 3D-Var and 4D-Var data assimilation techniques to two HPE events over central Italy, providing useful insights not only on the dynamical aspect, which can help us understand the local circulation, but also from numerical and applications aspects, relevant for modeling airflow over a complex physiography of central and southern Italy.

In this study, the physical mechanisms driving the development of the storm that occurred from 06 UTC to 13 UTC on 10 July 2019 along the central Adriatic coast of Italy are investigated by using numerical simulations, radar measurements, radio-soundings, and ground weather stations. The accumulated rainfall produced by the storm was approximately 127 mm in 3 h over the city of Pescara; also, giant hailstones

large about 14 cm in diameter caused extensive damage. Among the triggering mechanisms of this phenomenon the role of a cold front will be investigated.

The radar data and modeling simulations suggest that this event was a supercell (Montopoli et al., 2021; Tiesi et al., 2022), with the following characteristics:

- The storm moved offshore following the Italian Adriatic coastline.
- A strong thermal discontinuity was generated by the interaction of the bora wind with the warm and humid air preexistent over the central Adriatic Sea.
- The topography blocked the cold and dry northeasterly flow and drove a strong vertical wind shear in a deep layer (from 0 to 6000 m) along the coastline favoring supercell development.
- The SST supplied energy for storm maintenance.

The novelty of this study lies in the investigation of this exceptional storm and in the methodology used. The observations and very high-resolution (spatial and temporal) model outputs allow us to establish the most important physical mechanisms for supercell development and maintenance. The 3D structure of the cell will be discussed with further details in the companion paper (Ricchi et al., 2021

The paper is organized as follows: in Section 2 observations and numerical model experiments are presented; the meteorological characteristics of the event are discussed in Section 3; the model results in terms of dynamics and thermodynamics of the event are presented in Section 4; the sensitivity to the topography and to SST are presented in Section 5 and 6, respectively; conclusions are given in Section 7.

2. Observations and model

2.1. Observations

To investigate the structure of the storm, several categories of observations are used: satellites, radiosoundings, and ground-based data, such as weather stations and radar.

The ASCAT/OSCAT (Bentamy et al., 2012) scatterometer wind data a few hours before the hailstorm are used to investigate the bora jet associated with the frontal system traveling over the Adriatic Sea, which turned out to be a concurrent factor to the development of the storm cell. The SST data from satellite, limited area and global model outputs are used to investigate the role of the SST on the storm event. The network of meteorological stations, extracted from the DEWETRA platform (National Civil Protection), and weather stations managed by Regional Environmental Agencies of the affected regions, are used to investigate the evolution and the impact at the ground of the storm. To highlight the frontal passage along the coast and the associated weather parameters variations near the area affected by the hailfall, the weather station (Fig. 1 red dot) of "Pescara Porto" (42.46714°N, 14.2317°E) located in the harbor of Pescara, is used. Concerning heat flux data, and SSTs, the only available station data are from the harbors of Ancona, Pescara, and Ortona. Therefore, there are no observed data offshore; also, the three coastal stations are influenced by the presence of rivers and the geometry of the harbors, making the response to the mixing induced by the wind and the waves very slow. Therefore, the offshore SST is estimated based on the L4-level calibrated satellite data. To analyze the structure of the storm, data from the radar network of the Regional and National Agencies are used (Montopoli et al., 2021).

In particular, the two radars located on Mt. Il Monte (lon = 14.6208°, lat = 41.9394°, alt. = 710 m) and Mt. Serano (lon = 12.80017°, lat = 42.86594°, alt. = 1446 m) simultaneously observed the development of the supercell in a domain of the order of 100 km every 5 min at kilometer scale, thus allowing an in-cloud wind reconstruction (Montopoli et al., 2021). The radar data were accurately scrutinized in order to filter out unwanted signals (clutter, radiofrequency interferences etc.,) and some quality controls were applied in order to remove biases in the
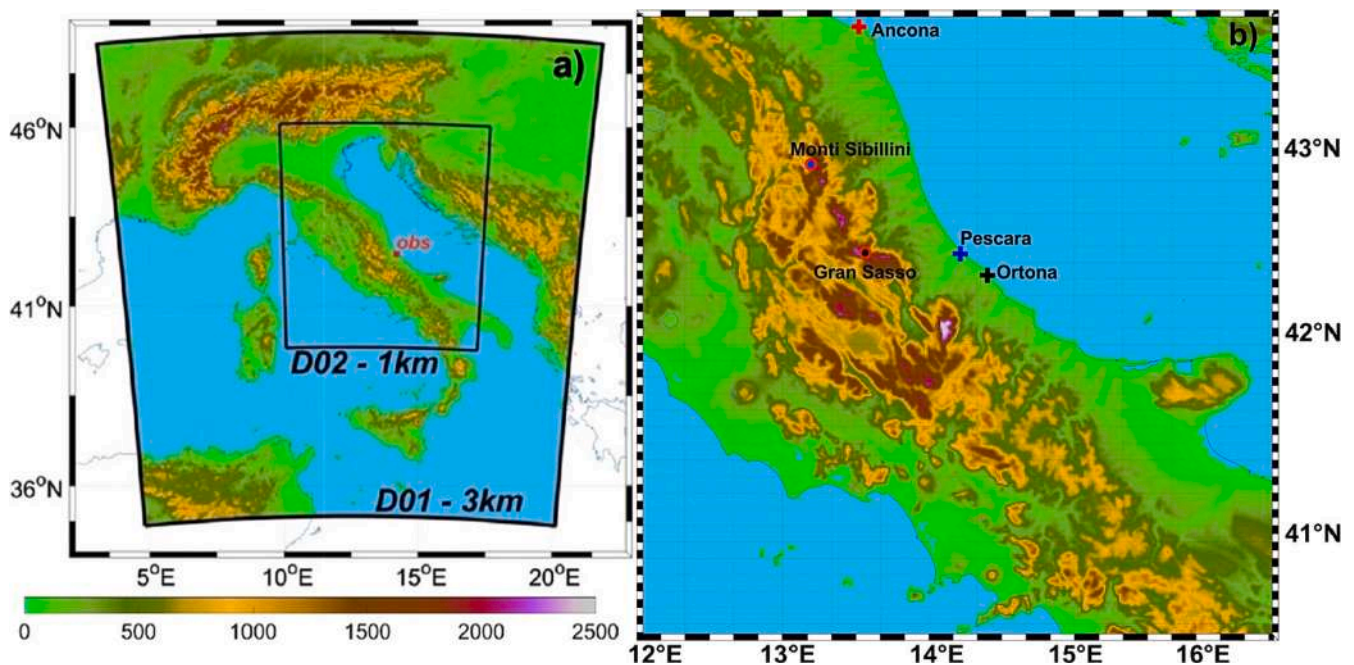
Fig. 1. Domains 1 at 3-km and domain 2 at 1-km grid spacing. Panel a) shows the model domains and topography (shaded, in meters), the red dot indicates the Pescara station; Panel b) shows the Mountain and the area of interest, location of weather station and referenced coastal cities impacted by storm. (For interpretation of the references to colour in this figure legend, the reader is referred to the web version of this article.)

measurement of the reflectivity factor. Since the supercell radar signature is quite isolated with respect to neighboring convective systems and the supercell-radar distance is limited (at the time of the mature phase, it is approximately 65 km), the corresponding signal to noise ratio at the radar receiver is quite high. Consequently, the supercell radar signature was very clear and its detection and tracking was easily performed manually as shown from Fig. 5a and the related caption.

2.2. Numerical model and experimental design

The Weather Research and Forecasting (WRF-ARW) numerical model version 4.0.2 (Skamarock et al., 2008) is used in this study. The model configuration is as follows: two two-way nested domains (Fig. 1 a, b) with the outer one, enclosing Italy with 3-km grid spacing, centered at 41.916°N, 12.47°E, and the nested domain centered over central Italy with 1-km grid spacing. To reproduce the triggering mechanisms, 110 vertical levels are used, the first level being located 15 m above the ground. The following parameterizations are used: the Mellor Yamada-Janjic (MYJ; Janjić and Janjić, 1994) for the Planetary Boundary Layer (PBL); the RTMM (Mlawer et al., 1997) and Dudhia (Dudhia, 1989) schemes for the longwave and shortwave radiation, respectively; the Milbrandt (Milbrandt and Yau, 2005) double-moment microphysics, which implements 6 classes of hydrometeors (Cloud, Rain, Graupel, Ice, Hail, Snow); the cumulus convection is explicitly computed on both

domains (Table 1). ECMWF analyses and 3-hourly IFS forecasts (Morcrette et al., 2009), with 9-km horizontal resolution, starting at 12 UTC on July 08, 2019, are used to initialise and driving the simulations respectively.

Several numerical experiments (Table 1) are performed with the aim of investigating the role of both SST and topography in triggering and enhancing the convective cell. This configuration is the result of these many experiments and was chosen after an extensive sensitivity study with a multi-physics ensemble approach (not shown).

1. (CTL) The Control run uses a MODIS native orography dataset and SST fields derived from the ECMWF-IFS initialization.
2. (NO_GS/ NO_GS & SM) To evaluate the impact of the orography, two sensitivity experiments are performed varying the height of the two highest peaks of the Apennines in Central Italy (Gran Sasso and Monti Sibillini). First, the Gran Sasso Mountain range is removed (NO_GS), then both the Gran Sasso and the Sibillini Mountains are removed (NO_GS & SM); hence, the maximum elevation in the modified area is imposed at 600 m. To prevent the discontinuity that may occur at the edges of the box (because the surrounding areas have an elevation higher than 600 m in Apennine Chain) the Shapiro-filter (Shapiro, 1970) is used with 16 smoothing cycles in the first 4 points that characterize the modified terrain. Using this approach,

Table 1
shows: the numerical configurations used for the sensitivity experiments, the names of the simulations (as used in the paper), the cumulus scheme (CU), the microphysics scheme (MP), the Planetary Boundary Layer (PBL) scheme, the soil scheme (SOL), the shortwave and longwave radiation scheme (Rad SW/LW), the dataset and the modifications that characterize the Gran Sasso massif (G. Sasso) and Sibillini Mountains (Sibillini), and the type of SST used in the runs, are indicated.

Simulation	CU	MP	PBL	SOL	Rad. SW/LW	G.Sasso	Sibillini	SST
CTL	Expl	Milbrandt	MYJ	Noah	RRTM/Dudhia	Modis 30s	Modis 30s	ECMWF
NO_GS	Expl	Milbrandt	MYJ	Noah	RRTM/Dudhia	removed	Modis 30	ECMWF
NO_GS & SM	Expl	Milbrandt	MYJ	Noah	RRTM/Dudhia	removed	removed	ECMWF
TOPOENHANC	Expl	Milbrandt	MYJ	Noah	RRTM/Dudhia	Realistic Peaks	Realistic Peaks	ECMWF
CMEMS_TOPO	Expl	Milbrandt	MYJ	Noah	RRTM/Dudhia	Realistic Peaks	Realistic Peaks	CMEMS 4 km
SST_HR_1km_TOPO	Expl	Milbrandt	MYJ	Noah	RRTM/Dudhia	Realistic Peaks	Realistic Peaks	GOS 1 km
SSTNOANM	Expl	Milbrandt	MYJ	Noah	RRTM/Dudhia	Realistic Peaks	Realistic Peaks	GOS 1 km–SST Anomaly (1985–2005)

the topography discontinuities that occur at the box boundary are smoother, preventing numerical noise and spurious dynamics.

3. (TOPOENHANC) A further simulation (TOPOENANCH) is carried out by adding the estimated difference in altitude between the MODIS 30s (MODIS Sciences Data Support Team) dataset and the ASTER (Advanced Spaceborne Thermal Emission and Reflection Radiometer; Abrams et al., 2020) maximum altitude of Gran Sasso and the Sibillini mountains, where at each point of the mountain

differences between the two datasets are added to obtain more realistic mountain peaks.

4. (CMEMS_TOPO) A few further experiments are performed with the aim of investigating the role of the SST combined with the enhanced topography. A simulation using a higher-resolution SST than in the CTL run (CMEMS_TOPO), derived from the Copernicus Monitoring Environment Marine Service (CMEMS; Clementi et al., 2017), is performed, as suggested by the results from previous works (Meroni et al., 2018; Miglietta et al., 2017a; Ricchi et al., 2019; Ricchi et al.,
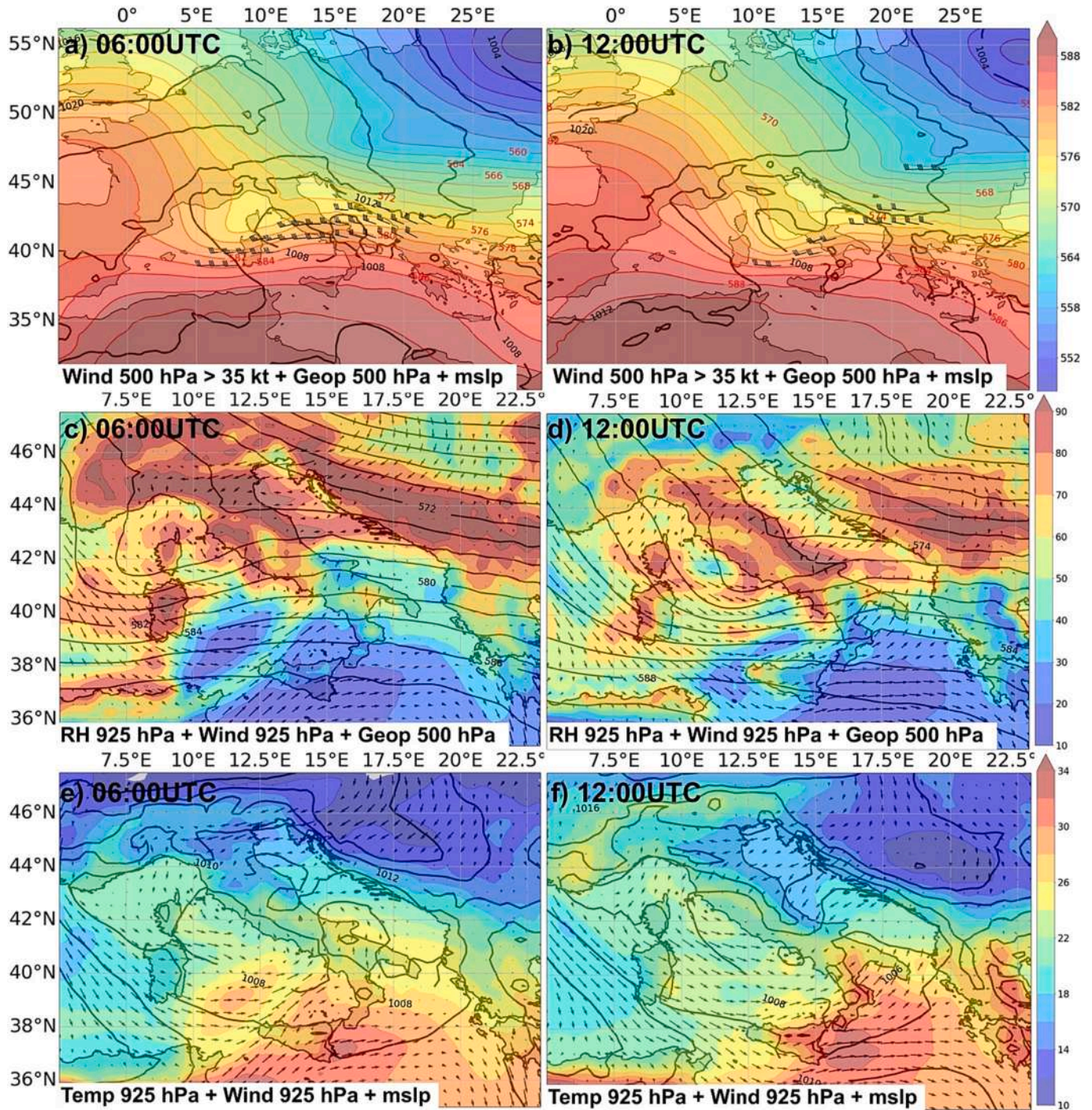

Fig. 2. a,b) Geopotential height at 500 hPa (red contours every 2 gpdm and shaded colour) and mean sea level pressure (black contours every 4 hPa), wind vector greater than 35 knots at 500 hPa (wind barbs), for 10 July 2019 at 06:00 UTC and 12:00 UTC, respectively. c,d) Relative humidity (shaded) and geopotential at 500 hPa (black contours every 2 hPa), wind vectors at 925 hPa. e,f) Temperature (shaded) and wind vectors at 925 hPa, mslp (black contours every 2 hPa), 06:00 UTC and 12:00 UTC, respectively. (For interpretation of the references to colour in this figure legend, the reader is referred to the web version of this article.)

n.d.). The CMEMS reanalysis dataset has 4.5-km horizontal resolution and is updated every hour.

5. (SST_HR_1km_TOPO) A further experiment is performed using a different dataset, i.e., the observed SST at 1-km resolution derived from Copernicus CNR-GOS group datasets (Nardelli, 2012).

6. (SSTNOANM) Finally, since the observed mean SST anomaly (Fig. 3a,b) over the Adriatic Sea is present during the event, a simulation is performed removing this anomaly from SST_HR_1km_TOPO. The anomaly field is taken from the same SST dataset, which also provides the SST anomaly, compared to a climatology for the 1989–2020 reference period (Nardelli, 2012).

All the numerical simulations are performed using the HAILCAST module (Brimelow and Reuter, 2009) to the aim of estimating the hail size at the ground. A deeper discussion of the module settings is presented in Ricchi et al., n.d..

3. Case study: Hailstorm on July 10, 2019

During the first ten days of July 2019, the Azores' high-pressure area expanded from the Atlantic Sea to northern Europe, advecting continental air masses toward the central and western Mediterranean Sea (WMS; Fig. 2a,b). The interaction between the WMS warm, wet air masses and the upper-level dry cold air, advected from higher latitudes, destabilized the atmosphere. At the same time, low pressure developed over the Balearic Islands, where a strong horizontal thermal gradient was present, and slowly moved southeastward advecting moist air toward central and northern Italy (Fig. 2c,d) and warm air toward southern Italy (Fig. 2e,f). Moreover, as the 500 hPa trough and the surface cyclone moved southeastward over the central Tyrrhenian Sea, cold advection affected the low levels in the northern and central Adriatic Sea (Fig. 2c,d), associated with an increase of northeasterly (Bora) winds. In this context, the SST showed a mean positive anomaly at basin scale of approximately +2.7 °C on the Adriatic Sea (SST ~ 26 °C), with a maximum of 4.4 °C reached off the Abruzzo coast; +6 °C on the Gulf of Lion, and + 4 °C on the Tyrrhenian Sea and the Strait of Sicily (with SST about 29–30 °C; Fig. 3a). Therefore, the incoming cooler air masses blowing over the warm sea favored the triggering of convective cells along the coastal areas. At the end of the event, the sea surface fluxes associated with the Bora outbreak were so strong that the SST anomaly was completely removed from the eastern side of the Adriatic Sea, where the SST anomaly became locally negative (Fig. 3b). Off the Abruzzo coast, where the storm developed, a + 3–3.5 °C SST anomaly remained, although smaller. The frontal passage lowered the SST anomaly by ~2 °C in this area and ~ 1.8 °C at the Adriatic basin scale.

The development of Bora jets in the northern and central Adriatic is well-known (Bergamasco and Gačić, 1996; Belušić et al., 2007 Belušić et al., 2013, Grisogono and Belušić, 2009; Davolio et al., 2017): the northern jets are the first to activate, then the central and southern ones (Cushman-Roisin et al., 2007; Belušić et al., 2007), turning into a surface cold front moving along the Adriatic basin from north to south. On July 10, 2019, the ASCAT detected a Bora jet in the morning (from 08:30 UTC to 09:44 UTC) in the northern Adriatic Sea with gusts reaching 30 kt and another one in the central Adriatic Sea (Fig. 4a-c) with gusts exceeding 35 kt.

The Italian radar network detected a multicellular thunderstorm north of Pescara, along the coast between 08:30 and 09:00 UTC (Fig. 5a, b), moving from the Marche to the Abruzzo region. The storm was characterized by three main cells with VMI values reaching 50 dBZ (see Fig. 4 in Montopoli et al., 2021). The storm moved southward along the coastline, and extended offshore, showing several intensification phases (Fig. 5c,d). Between 09:50 UTC and 11:00 UTC, the storm reached its peak intensity, with a VMI of 60–65 dBZ, near Pescara (Fig. 5e,f). Concurrently, an additional cell developed farther offshore.

The storm caused heavy rainfall in the coastal area of Pescara between 09:00 UTC and 11:00 UTC. The "Pescara Porto" weather station recorded approximately 127 mm in 3 h with the maximum hourly rainfall reaching 110 mm/h between 10.30 UTC to 11.30 UTC (Fig. 6c). The rainfall spatial distribution shown in Fig. 6a suggests the trajectory of the storm that moved along the coast and reached its maximum intensity in the coastal area near Pescara. A remarkable characteristic was the presence of an intense hailstorm over the city of Pescara with giant hailstones reaching 14 cm in diameter, described by European Severe Weather Database (ESWD) (Dotzek et al., 2009). Moreover, as the front crossed Pescara station, a sudden decrease in temperature of approximately 8 °C was recorded (Fig. 6b); as the cold front moved away from this area, the SST anomaly drops by 0.9 °C in the Adriatic sea after the frontal passage (Fig. 3b).

The Italian weather station data of temperature and relative humidity at 2 m, wind speed and direction at 10 m (Fig. 7a-f) are used to analyze the evolution of the air masses in this event. The data are
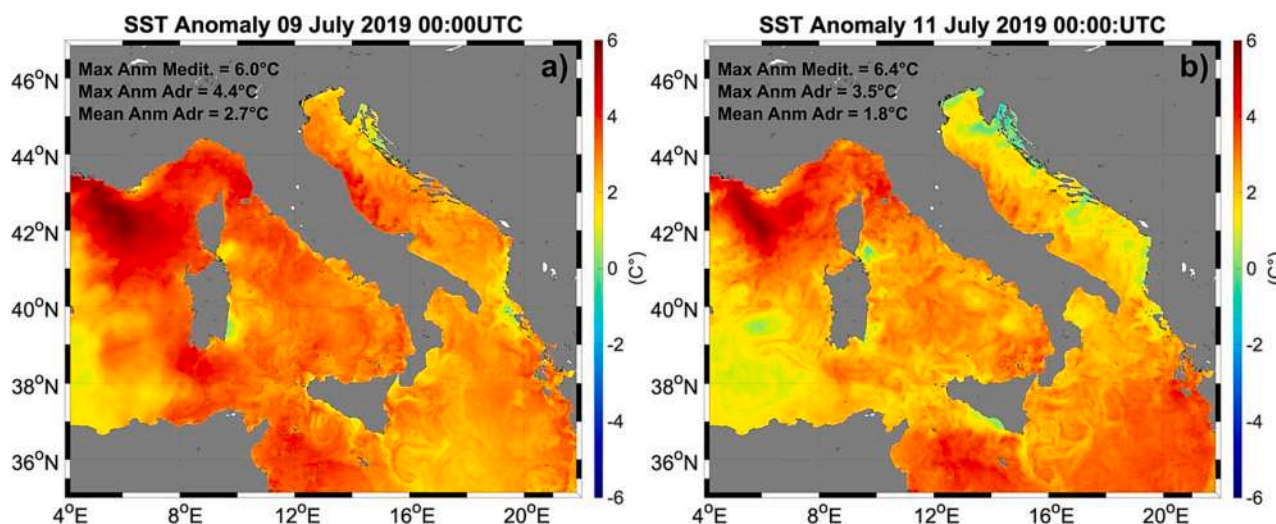

Fig. 3. Sea Surface Temperature (SST) Anomaly with respect to the 1985–2005 climatology, data from Copernicus Marine Services, SST Anomaly field in the dataset Mediterranean Sea High Resolution and Ultra High Resolution Sea Surface Temperature Analysis (Nardelli, 2012); a) at 00:00 UTC July 09, 2019 before the storm; b) at 00:00 UTC July 11, 2019 after the cold front passage. On the upper left side are shown the maximum values of SST anomaly in the Mediterranean basin and Adriatic sea, and the mean SST anomaly over the Adriatic sea (before and after the storm).
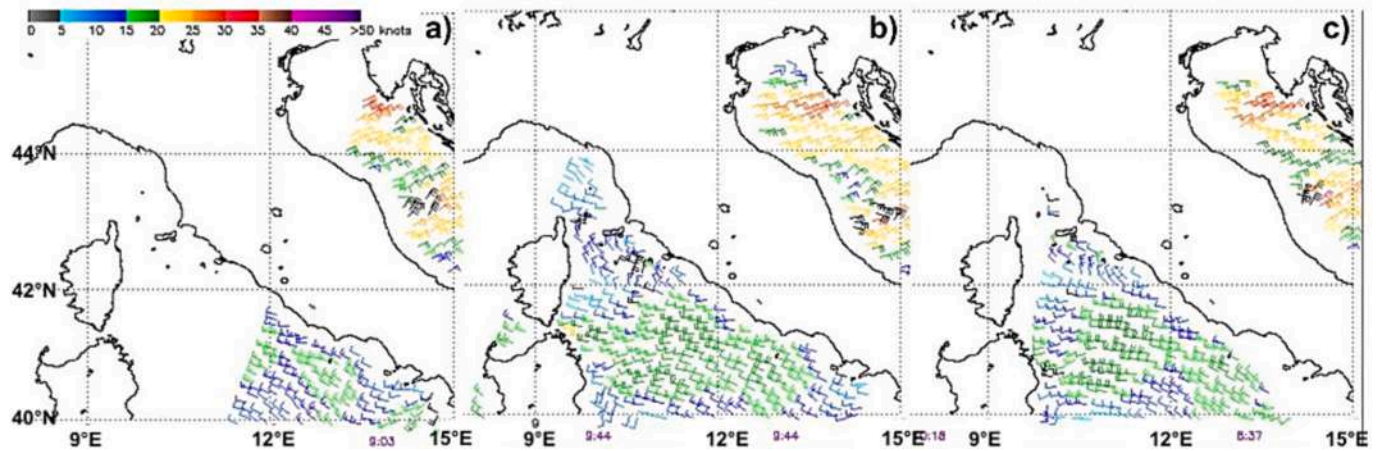
Fig. 4. Wind speed and direction from ASCAT MetopA/B satellite (https://www.remss.com/missions/ascat/) on July 10, 2019, at the time in the lower right part of the figure; wind speed in the colour bar (in knots). Black barbs, near the Italian Adriatic coast, are nearby the rainfall area.
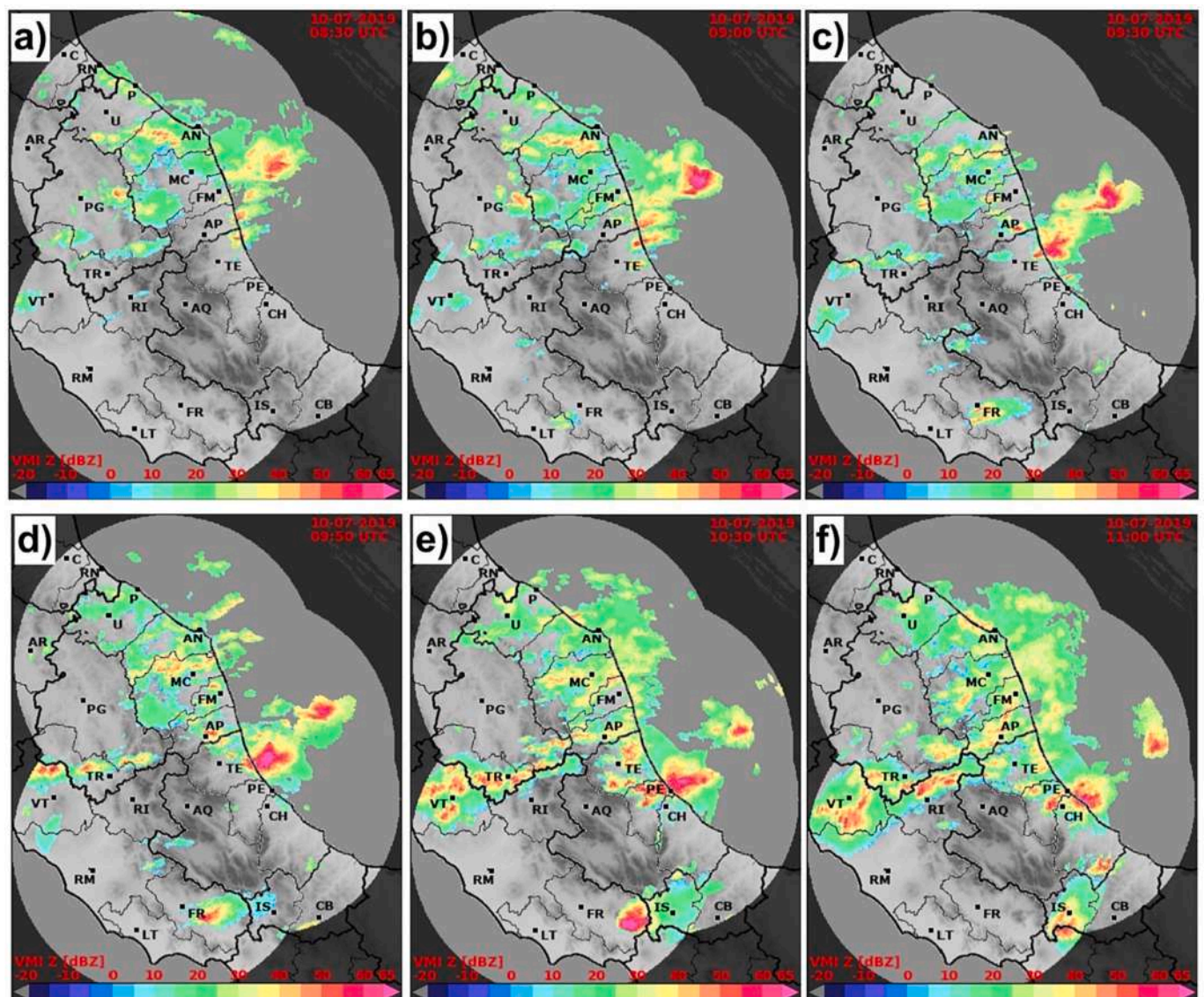

Fig. 5. The radar reflectivity (dBZ) at: a) 08:30 UTC, b) 09:00 UTC, c) 09:30 UTC, d) 09:50 UTC, and e) and f) at 10:30 UTC and 11:00 UTC respectively, during the phase when the storm hits the city of Pescara, and generates the intense hailstorm, at the times of 10:30 and 11:00, respectively.
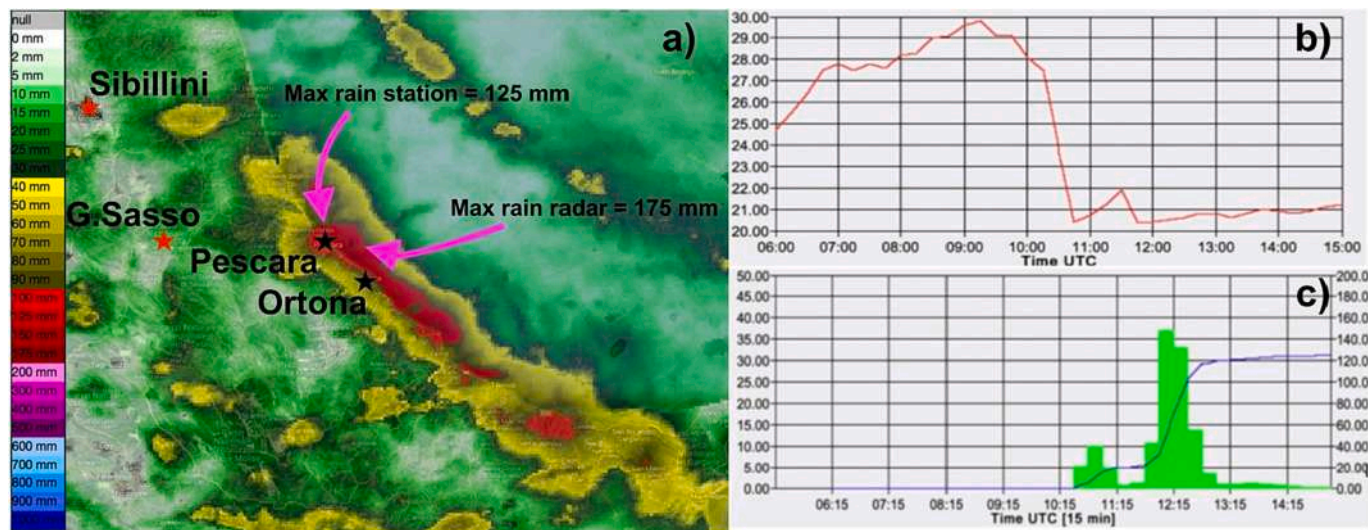
Fig. 6. Interpolated weather station data from DEWETRA (Parodi et al., 2010): a) accumulated rainfall (hourly data) from 09:00 to 10:00 UTC on July 10, 2019; b) time series of 2 m temperature (10 min data frequency) at Pescara station; c) time series of hourly accumulated rainfall at Pescara Porto.
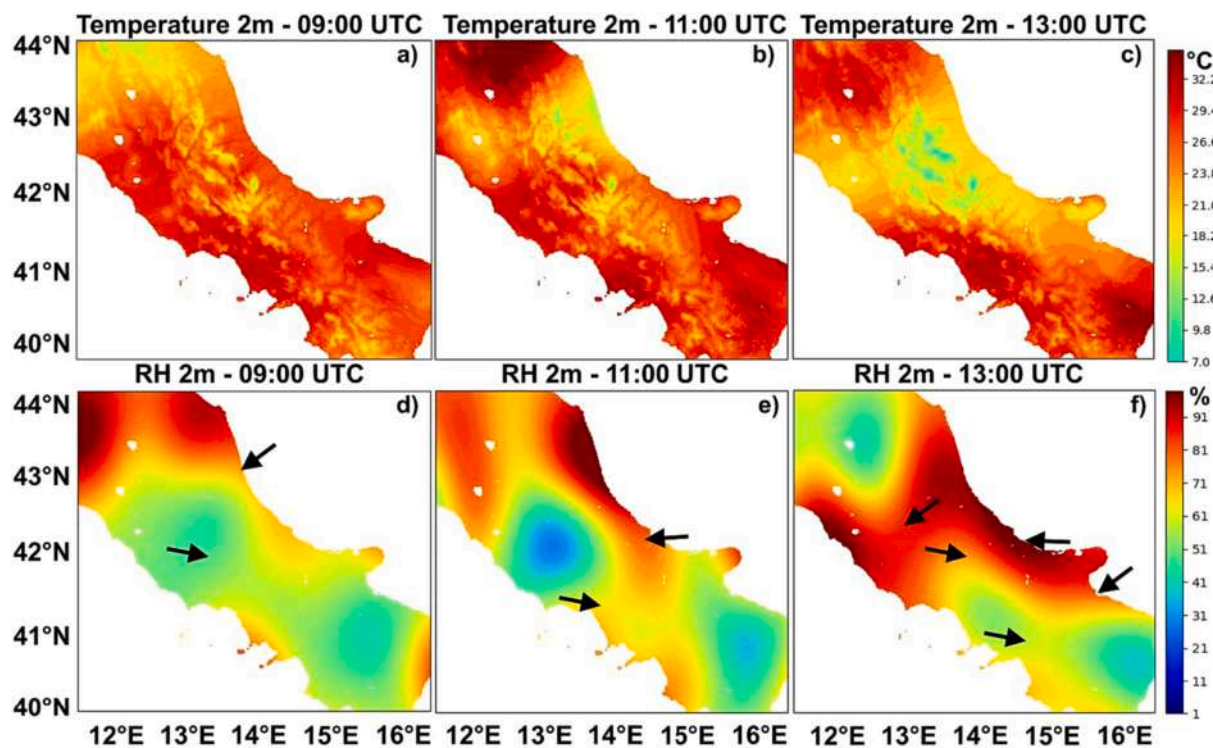

Fig. 7. Hourly time evolution at 09:00, 11:00 UTC, 13:00 UTC of the interpolated: a.c) Temperature at 2 m; d-f) relative humidity at 2 m; vectors represent wind direction taken from the official weather station dataset.

horizontally interpolated over the grid and topography taken from the WRF model; the adiabatic gradient is calculated in the first 3500 m of the atmosphere, from the radiosoundings of Pratica di Mare (41.65 N, 12.43E) and Zadar (44.10 N, 15.34E). Stations data are provided by the DEWETRA web portal (Parodi et al., 2010).

The bora jet blowing from the northeast (Fig. 7d-f) and moving from north to south along the Adriatic coast advected cold and humid air toward the Apennines.

Finally, the Rapid Scan High Rate SEVIRI shows (Fig. 8a-f) the time evolution of the storm in the Adriatic Sea. Between 09:30 UTC and 11:00 UTC the cell is clearly in the growth phase (Fig. 8a-d), as SEVERI shows a rapid increase of the cell extent and a reduction of the brightness

temperature to a very low value ($\sim -60/-70\ °C$), suggesting the presence of a high-top cloud and strong ascending motion, as indicated by the typical U-shaped structure. Moreover, the lowest value of the brightness temperature is reached approximately over Pescara (Fig. 8 a-f white dot in the center of the storm cell) suggesting a very localized and a very deep storm cell.

The following questions will be addressed in the rest of the paper: whether it was a supercell, how it formed, and what caused the development of huge hailstones. Therefore, to better investigate the vertical structure of the cell, its time evolution and what triggered the formation of this extreme event, numerical simulations are analyzed.
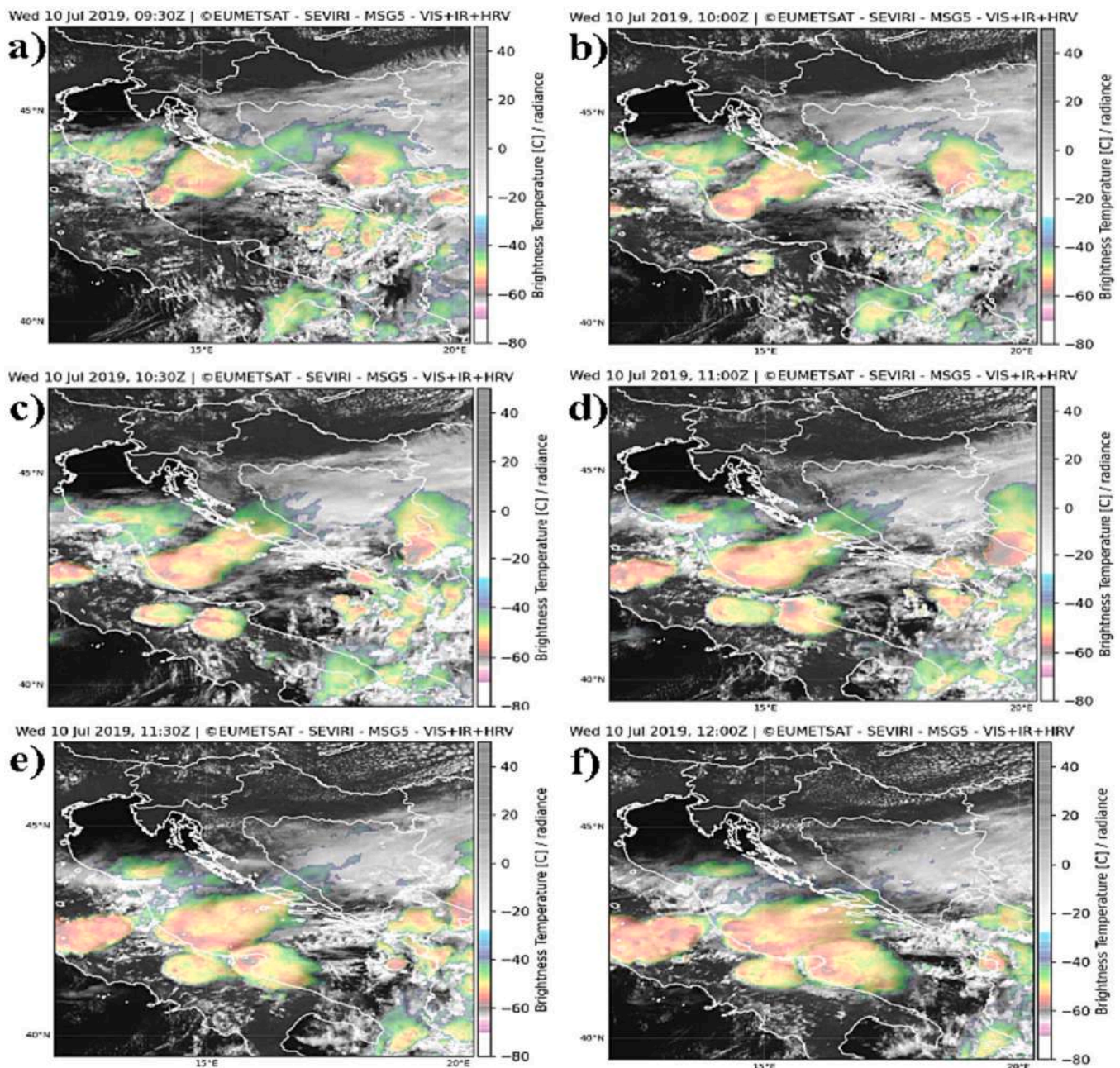
Fig. 8. Visible and infrared channel and brightness temperature 10.8 channel of the EUMETSAT-SEVIRI dataset at a) 09:30 UTC July 10, 2019, b) 10:00 UTC July 10, 2019, c) 10:30 UTC July 10, 2019, d) 11:00 UTC July 10, 2019, e) 11:30 UTC July 10, 2019 and f) 12:00 UTC July 10, 2019.

4. Dynamics and thermodynamics of the storm: Model results

In this section, dynamics and thermodynamics of the storm are analyzed at the basin and local scale. The SST_HR_1km_TOPO results are taken as a reference because of the improvement in the accumulated rainfall with respect to the CTL simulation. Vertical cross sections are taken in different geographical areas (all near Pescara) to track the storm cell. The SST_HR_1km_TOPO reproduces the storm with reasonable accuracy in terms of time evolution, intensity, and location (a detailed intercomparison of the simulations is provided in Ricchi et al., 2021). Indeed, the evolution of the phenomena simulated by the SST_HR_1km_TOPO is comparable with the radar data observations. Three air masses, originating from different areas, contribute to the storm development (Fig. 9 a-d). The cyclone in central Italy (Fig. 2 a-f) advects warm humid air from southeast and cool dry air from the

northeast; as the cyclone moves southeastward it triggers the Bora jet from the Balkans.

The first airmass (AM1), which is associated with the Bora jets coming from the Balkans, is initially located on the north-central Adriatic (Fig. 4b) and then moves southward, as shown in Fig. 9a-c. During the hours before the event, between 08:40 and 09:40 UTC, AM1 is relatively dry and cold with an equivalent potential temperature $\theta_e = $ 50–55 °C at 1000 hPa and a depth of $\sim$1000 m (Fig. 10 d-e). An increase in humidity occurs as AM1 crosses the Adriatic Sea, with RH increasing from 40% near Croatia to 65–70% as it approaches the Italian coast. A representative simulated sounding from this airmass at 09:00 UTC (Fig. 10a) shows a stable profile for AM1 (43.5°N, 14.5°E) with no CAPE, high values of Precipitable Water (PW) of 40 kgm^{-2}, Lifted Condensation Level (LCL) of $\sim$900 m and a Showalter Index (i.e., an estimate of the air parcel instability at 850 hPa: negative values represent unstable
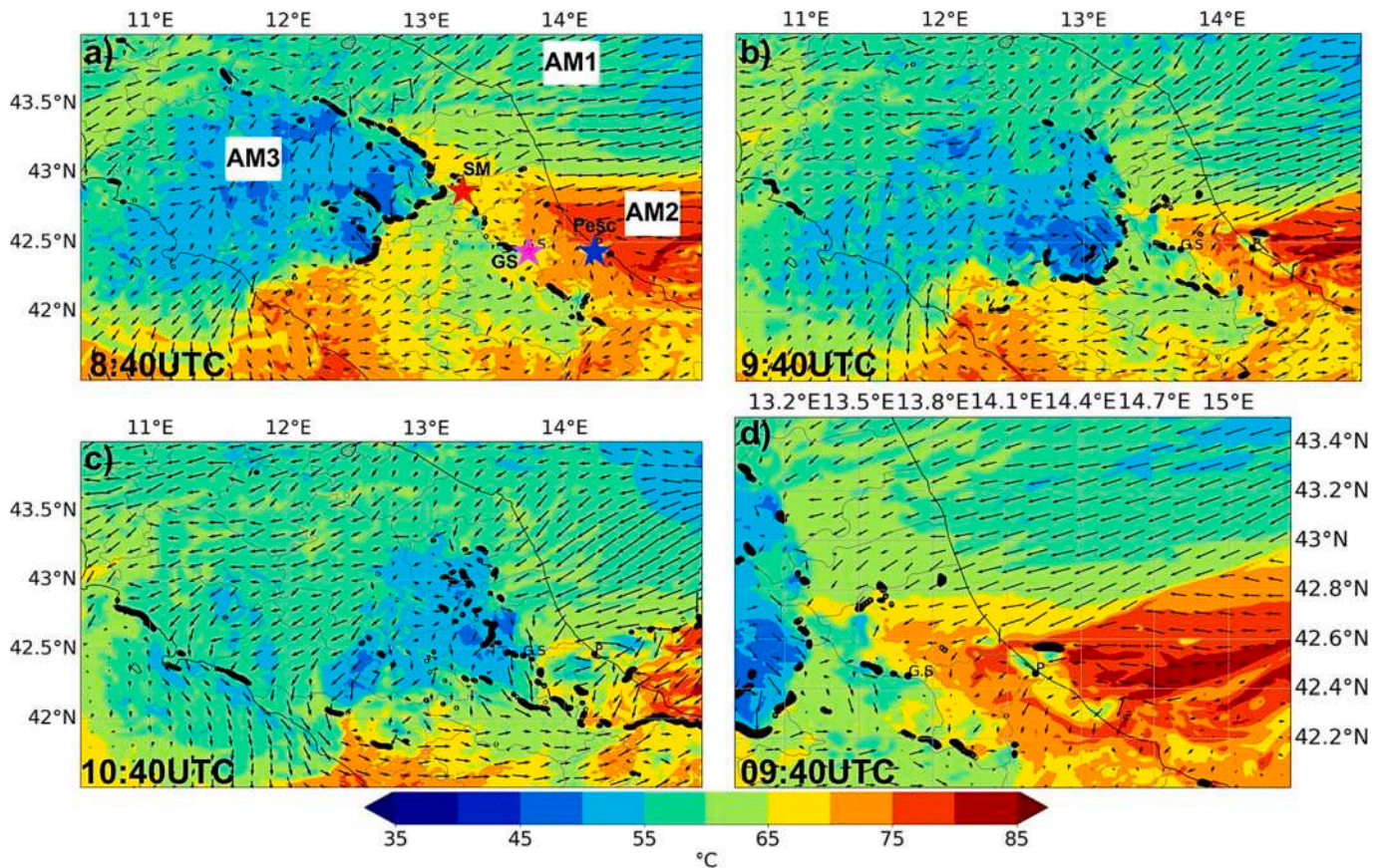
Fig. 9. Panels (a-c): equivalent potential temperature (θ_e shaded in °C) and wind speed and direction at 1000 hPa. The geographical area of interest is central Italy at 08:40 UTC, 09:40 UTC and 10:40 UTC. Panels (d) zoom in the storm-development area at times 9:40 UTC. AM1, AM2, AM3 are respectively the different airmasses, associated with the cold Bora from the Balkans (AM1), the preconditioned area present in situ over the Adriatic Sea before the event (AM2) and the cold, dry pool (AM3) generated over the Apennines and driven by the movement of the low-pressure area. The red star indicates the location of the Sibillini Mountains, the purple star indicates the location of the Gran Sasso Massif and the blue star indicates the position of Pescara. (For interpretation of the references to colour in this figure legend, the reader is referred to the web version of this article.)

air columns, values between -4 °C and -1 °C are typical of marginal instability, less than -4 °C suggest strong instability, calculated using *Showalter Index* = T_{env} - T_{parcel}) of approximately -1 °C (weakly unstable air).) The value of the midlevel vertical wind shear (0–3000 m) is around 8 ms^{-1} with a maximum reaching 10 ms^{-1}. As AM1 crosses the Adriatic Sea, it interacts with the SST reaching 28–29 °C near the Italian coast. Consequently, heat fluxes exceeding 2200 Wm^{-2} in the area upstream of the storm (not shown) are simulated. As shown in Fig. 10d-e, the bora jet is limited to the first 1500 m above the ground, showing an undulating movement, typical of the bora jets. The oscillation is produced by the turbulent heat flux which induces heat and moisture transfer from the sea, turning into an increase of CAPE, and slightly increases the air pressure and the PBL thickness. According to this mechanism, the low-level airmass speeds up and experiences an increase of humidity (O'Neill et al., 2003, 2005, 2010) as it reaches the Italian coasts. Then AM1 penetrates inland and intrudes below the other airmass AM2, pushing it upward (Fig. 10d-e). As shown in the sounding (Fig. 10a), AM1 is wet at the low levels up to 1500 m, becoming drier above, which is a characteristic of the Bora. Between 1500 and 3000 m, the air mass over the Adriatic is characterized by a tongue of warm and humid air extending over the sea from the west (AM2, Fig. 10 d-e and Fig. 10 f-g). Hence, a strong vertical wind shear is found between 1500 and 2000 m because of the inversion in wind direction. At upper levels, between 5500 and 7000 m, a cold and relative dry air mass coming from northwest is found (Fig. 10a).

The cyclonic circulation located in the central-southern Tyrrhenian Sea produces an easterly flow of warm and moist air between the surface

and 3000 m toward the central-southern Adriatic, which corresponds to the second airmass (AM2). AM2 is characterized by a thickness of ~2500 m, θ_e = 75 °C at 1000 hPa, 2 m Rh = 90–95% (Fig. 10b and f-g). The vertical sounding at (42.525°N, 14.469°E) shows that CAPE exceeds 4500 JKg^{-1}, PW = 50 Kgm^{-2}, LCL is located at approximately 970 hPa where the temperature reaches 23 °C, and LFC is close to 500 m, so that even a small uplift is sufficient to trigger convection. The Showalter index (SHOX) reaches -4 °C, confirming a high potential for thunderstorm development (the sounding is taken near the storm cell, just offshore of Pescara), and wind shear between 0 and 3000 m of 10–12 ms^{-1}, corresponding to a moderate-to-high midlevel shear. AM2 penetrates inland reaching the Apennine chain, as shown in Fig. 9a-d.

In the meantime, AM1 enters inland pushing AM2 toward the Apennines southeastward. At lower levels (0-1000 m), AM1 acts as a dense cool pool, pushing AM2 upwards along the convergence line.

The third air mass (AM3) is associated with the cold front that is moving from the central Tyrrhenian Sea to the southern Adriatic Sea (Fig. 2, Fig. 7, Fig. 10c and Fig. 11a-d). This air mass moves eastward at a mean speed of 14–16 m s^{-1} and has a thickness of about 4500–5000 m (Fig. 11), and at the surface θ_e = 40 °C is associated with the coldest part of AM3. A sounding at 42.3°N, 12.75°E shows CAPE close to 2141 JKg^{-1}, PW approximately 20 kg/m^{-2}, LCL located at 860 m height with a temperature of 16 °C, and the SHOX index of +3. Between 09:00 UTC and 10:30–10:40 UTC, AM3 interacts with the Apennines, mainly with the Sibillini and the Gran Sasso Mountains (Fig. 9c and Fig. 11a-d): the low-level blocking allows only the upper air to cross the mountains and to pass over AM2 above 3000 m, making the air column over the sea
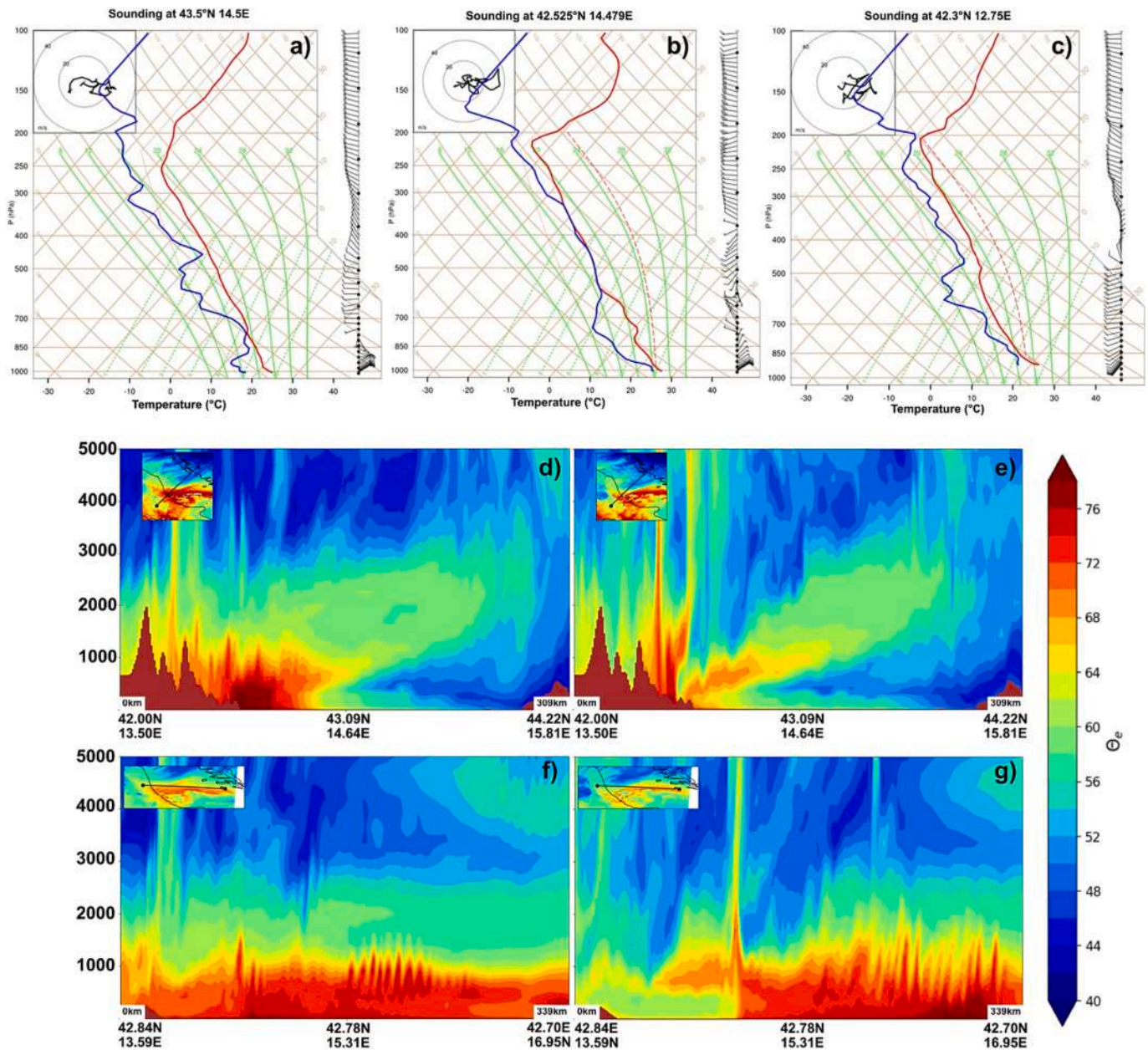
Fig. 10. Panels a-c, simulated radio soundings (at refered coordinate reportend in upper side of panel a-c) at 09:00 UTC in the areas affected by the air masses AM1 (panel a) latitude 43.5° N longitude 14.5°E, AM2 (panel b) latitude 42.525°N longitude 14.479°E, AM3 (panel c) latitude 42.3°N longitude 12.75°E. Panels d-e represent the vertical sections of θe, for AM1 at 09:00 UTC (panel d) and 10:00 UTC (panel e). Panels f-g show, at the same times, the θe cross section (°C) for AM2.

unstable (Fig. 11c-d). The supercell development is favored by the strong wind shear between the lower and the upper layers: above AM2, between 0 and 6000 m, the wind shear is greater than 100 kt, whereas along the frontal system in the lee (western) side of the Apennines reaches 70–80 kt (as shown in figure Suppl_2). The blocking prevents the dense part of AM3 (around 925 hPa) from flowing along the coast and affecting the formation of the cell, as will be shown in the following section. This highlights the dual role of the topography, which blocks the cold and very dense lower-layer air at 925 hPa, drives the upper part of AM3 above AM2, and helps the development of strong convection (Fig. 12a-d) with vertical velocities larger than 20–30 m s^{-1}.

Convection is triggered at the convergence line between AM1 (moving southwestward at 16–20 m s^{-1}) and AM2 (moving northwestward at 12 m s^{-1}), (Fig. 12 d and h), so that the air is lifted above the low (600 m) LFC. At this stage, from 9:40 UTC to 10:10 UTC, large vertical velocities are reached with values exceeding 12 ms^{-1} at the height of

2500 m. Furthermore, as shown in Fig. 12, the vertical structure of the storm, with vertical speeds greater than 45–50 ms^{-1}, from 6 km to up-to 15 km, is consistent with that observed and described in Montopoli et al., 2021.

In fact, the maximum content of graupel, snow, and ice is reached between 5000 and 11,000 m (Fig. 12c). The SST_HR_1km_TOPO shows very intense CAPE along the trough, with the edge reaching the storm maximum intensity area close to Pescara, with CAPE up-to 4000 JKg^{-1}, and maximum size of the hailstones close to 70–90 mm (Figure Suppl 3). Both the maximum observed (estimated) diameter around 100–150 mm and the simulated maximum accumulated rainfall (138 mm) are in good agreement with the observations both in amount, time, and space. The maximum precipitation is located very close to Pescara (Fig. 13, blue triangle; Montopoli et al., 2021) with the axis and the anvil perpendicular to the coast forced by the upper layer wind, whereas the path of the cell along the coast is driven by the frontal system evolution, as
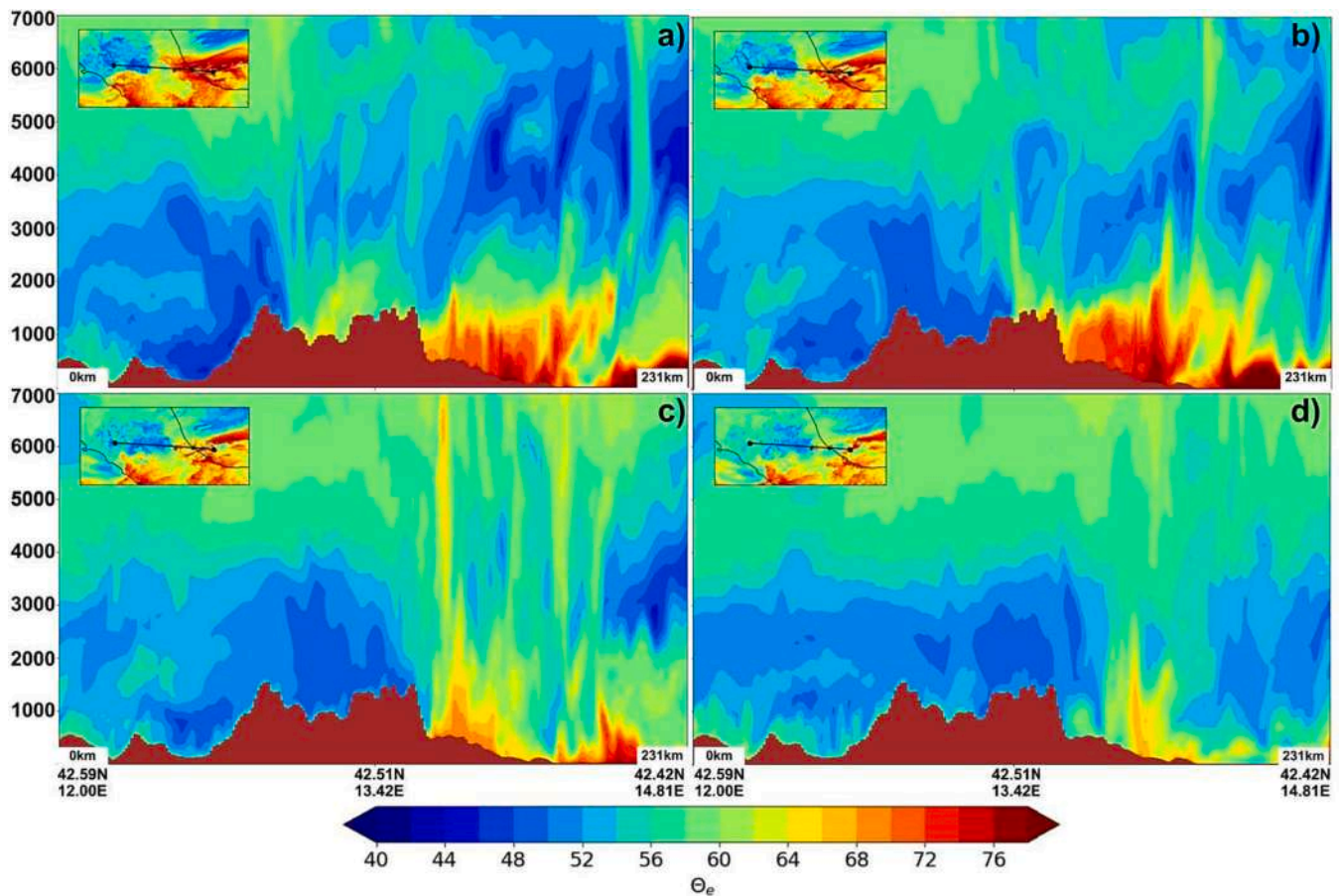
Fig. 11. Panels a-d show the vertical sections of θe for AM3 (and part of AM2 in the storm development area) from 09:00 UTC (panel a) to 10:30 UTC (panel e) every 30 min.

previously described.

In summary, the development of the storm is strongly driven by the cold pool produced by AM1, which rapidly spreads over the Adriatic Sea from north to south following the coastline. Moreover, the characteristics of air masses and their interaction with the topography are very important for the development of the storm (Rotunno et al., 2017), as shown for AM2 and AM3 whose movement is affected by the Sibillini and the Gran Sasso ridges. Moreover, the speed and direction of Bora jets are modulated by the SST, which controls the air-sea interaction, as discussed in Ricchi et al. (n.d.), Meroni et al. (2018), Cassola et al. (2016), and Miglietta et al. (2017a). In this event, the orography 'guides' the air masses: AM2 is blocked and forced to rise at the upper layers;

AM1 (Bora Jet) moved inshore southward; AM3 is partially blocked by the Apennines and partially forced to flow above the other two air masses, producing a strong vertical wind shear. In this scenario, it can be hypothesized that even a small perturbation of these two parameters, the SST and/or the orography, can largely impact the development of the supercell. Therefore, a sensitivity study of both components is presented in the next sections.

5. Sensitivity to the orography

The effects of the orography are investigated by means of a few numerical experiments (Table 1);

1) a first experiment in which the Gran Sasso Mountain is removed (NO_GS);
2) the second one in which the Sibillini Mountains are also removed (NO_GS & SM);

3) in the last one the difference between the model orography and the real elevation of the peaks of the two mountains is added to the model orography (TOPOENHANCE). With the aim of highlighting the role of the topography, the same SST is used (from ECMWF analysis) for all these sensitivity experiments. Some metrics are used to assess the quality of the simulations, and they are in Table 2. These indices are calculated by tracking the updraft of the convective cell and comparing it with the result provided by radar (maximum reflectivity) and satellite (position of the overshooting top) observations. In detail MAR is the maximum accumulated precipitation, and it consists of the total cumulative precipitation from the storm, keeping in mind that the simulated cumulative precipitation from other precipitation events not related to the supercell event is discarded. TDMS is the Timing Differences of Maximum Storm Development and is calculated as the maximum difference between the observed maximum storm intensity (radar data, rainfall) and simulated maximum (rainfall). MHA Maximum Hail Accumulated, which is the maximum amount of hail accumulated during the supercell event (following the estimate made for rainfall), and MSD Mean Storm Distance which is the geometric mean distance between the observed (with radar) and simulated cell location, in space and time.

A preliminary comparison among the experiments is performed in terms of cell position and intensity. The distribution of total accumulated rainfall (Fig. 6a) and hourly accumulated precipitation from 06:00 UTC to 13:00 UTC (the entire duration of the phenomenon along the Adriatic coast) shows a strong sensitivity to the orography (Fig. 13a, c, e, g): when the Gran Sasso mountain is removed (NO_GS) no large variation is found in the maximum intensity (Fig. 13c), since a small
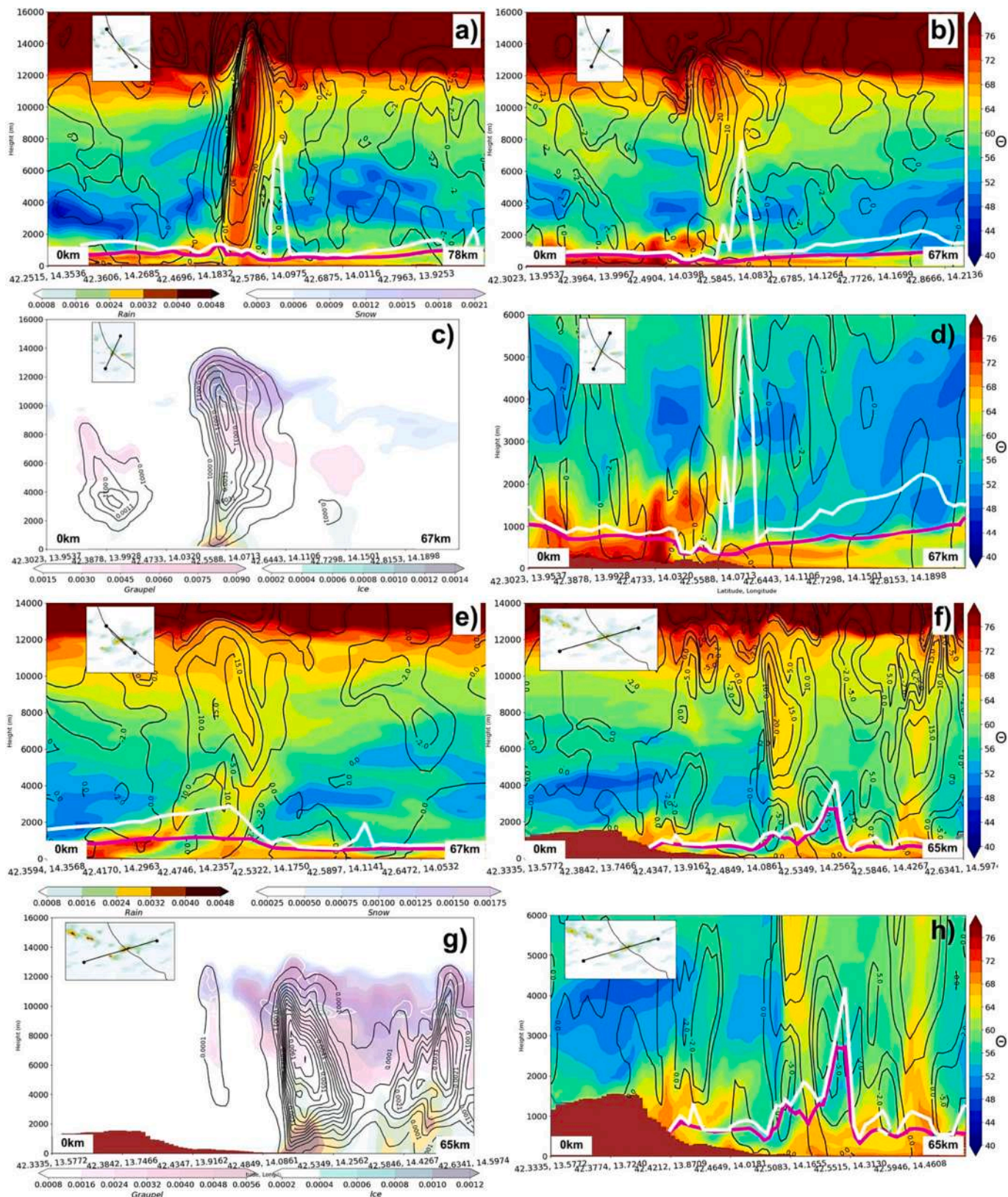
Fig. 12. SST_HR_1km_TOPO simulation: (a) θe (shaded), vertical velocities (m s^{-1}, black lines), LFC (m, white lines) and LCL (m, magenta lines) at 10:00 UTC along a transect parallel to the coast; b) as in a) but along a cross-section of the cell perpendicular to the coast and to the storm movement; c) mixing ratio for hydrometeors (kg kg^{-1}): Snow, Ice, Graupel, Rain (colour code) and Hail (contours) at 10:00 UTC; d) as for b) but for a zoom reaching only 6000 m of elevation; e) to h) as for the previous set but at 10:20 UTC, the time of the maximum intensity of the phenomenon. (For interpretation of the references to colour in this figure legend, the reader is referred to the web version of this article.)
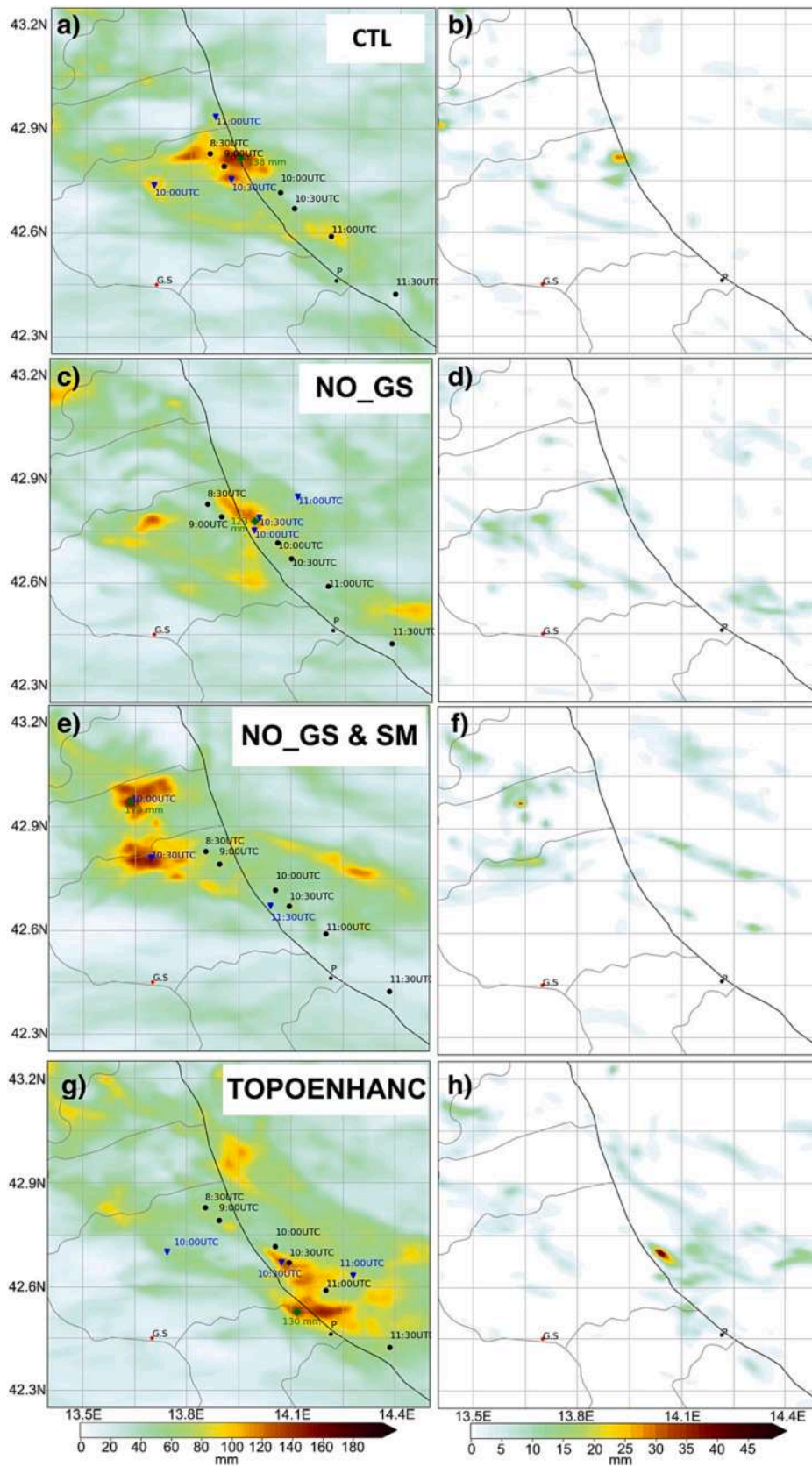
(caption on next page)

Fig. 13. The distribution of accumulated precipitation from 06:00 UTC to 13:00 UTC for: a) CTL, c) NO_GS, e) NO_GS & SM and g) TOPOENHANC. The black dots indicate the position and time of the storm cell (maximum reflectivity) obtained from the radar (Montopoli et al., 2021). The blue triangles show the position and time of the maximum rainfall recorded at the same times as the radar data. The observed maximum accumulated precipitation during the storm is shown in green. The analysis is carried out by taking into consideration only the area around the storm cell, from its development to its extinction. Panels b, d, f and h show the accumulated hail on the ground from 06:00 UTC to 13:00 UTC. (For interpretation of the references to colour in this figure legend, the reader is referred to the web version of this article.)

Table 2

Differences between all simulations, in terms of: Accumulated Rainfall (MAR); Timing Differences of Maximum Storm development (TDMS); Maximum Hail Accumulated (MHA), Mean Storm Distance (MSD, radar vs simulation, in km every 30 min).

	MAR (obs 127 mm)	TDMS	MHA	MSD
CTL	138 mm	−30 min	27 mm	27 km
NO_GS	123 mm	−45 min	20 mm	18 km
NO_GS & SM	173 mm	−60 min	37 mm	31 km
TOPOENANCH	130 mm	−15 min	40 mm	21 km
CMEMS_TOPO	144 mm	+20 min	10 mm	15 km
SST_HR_1km_TOPO	127 mm	−20 min	12 mm	10 km
SSTNOANM	165 mm	−20 min	47 mm	33 km

reduction of the MAR (maximum accumulated precipitation) 127 mm (observed) 138 mm (simulated), is found together with a secondary maximum further inland. Also, the horizontal extent of the area affected by the most intense rainfall is significantly reduced. On the other hand, a larger sensitivity occurs when both the Gran Sasso and the Sibillini Mountains are removed (Fig. 13e): the MAR (maximum accumulated precipitation) 173 mm, overestimated and located inland; also, a secondary maximum of comparable intensity is identified inland (Table 2). This suggests the onset of a channeling of the low-level easterly flow by removing the two ridges, emphasizing that both mountain ridges play a key role in the location and intensity of the precipitation by forcing the rainfall to occur along the coast. The last experiment is performed by correcting the elevation of the two peaks to the real values.

A large impact on the location and amount of accumulated rainfall is found for TOPOENHANC (Fig. 13g, h), since the MAR is slightly underestimated (130 mm) but its position near Pescara is in good agreement with the radar observation. Moreover, the hail accumulated at the surface reaches 40 mm. Because of the sensible impact on the accumulated rainfall of either removing or enhancing the mountain ridges, the impact of the latter on the dynamics of the storm is briefly described in the following sections. For brevity in this discussion, only the figure related to the TOPOENHANC experiment is shown, because this configuration will be used in the following analysis.

5.1. Removing the Gran Sasso only and both Gran Sasso and Sibillini mountains

The results of the simulations performed removing only the Gran Sasso mountain (NO_GS) and then both the GS and Sibillini (NO_GS & SM) are now discussed. For the NO_GS experiment, before the event the humid and warm air mass AM2 penetrates inland flowing through the gap due to the lack of the Gran Sasso mountains. The cold pool (AM3), which is blocked by the Sibillini and Gran Sasso mountains in the CTL, splits into two parts: one speeds up through the gap and reduces the westward propagation of the unstable air coming from the sea. The other branch of the cold pool turns around the Sibillini Mountains and approaches the sea triggering convection (not shown).

The impact of the highest peaks of Abruzzo and Marche regions is investigated by removing both Gran Sasso and Sibillini mountains (NO_GS & SM). The dynamics of the event strongly change in this simulation (Figure Suppl_1): the unstable air mass (AM2) penetrates inland reaching the Apennines while the cold pool (AM3) is not blocked by the mountains, and it flows along the coast extending to the southeast. Hence, AM3 approaches both AM1 and AM2 further inland, where

a convective cell develops within the convergence line (Fig. 13 and Table 2, TDMS and MSD values).

5.2. Enhancing the topography (TOPOENHANC)

Comparing the WRF topography with the real orography, large differences are found: an underestimation of the main peaks of the Gran Sasso Mountain and the Sibillini Mountains, up to 400–600 m, is found (not shown). To investigate how the highest peaks of the Apennines impact the dynamics and thermodynamics of these coastal events, a correction point-by-point is applied to the WRF topography at the grid points showing an underestimation. The TOPOENHANC shows large similarities with the CTL, but local differences are observed for the whole simulation. Between 09:00 UTC and 09:30 UTC, an increase in the zonal speed of AM3 is found downstream of the Sibillini mountains, together with a decrease of θ_e by 5 °C with respect to CTL. Moreover, the convergence line between AM3 and AM2 along the coast is stronger and develops earlier (i.e., it is faster) than CTL. This produces a southward displacement of AM2 turning into a lack of the energy contribution, in CTL run, necessary for sustaining convection when AM1 approaches the coast. The TOPOENHANC run shows a more intense and persistent zonal propagation of the convergence line (Fig. 14a-c) than the other simulations. At 10:00 UTC there is still a tongue of AM2 that climbs up to the slopes of Gran Sasso with $\theta_e = 70$ °C (Fig. 14b-c). Between 10:10–10:20 UTC the convergence line continues to intensify along the coast, weakening and shifting AM2 southward. At this stage, CAPE is larger than 4000 JKg^{-1} and the most intense precipitation is produced: the 3-h accumulated rain reaches ~130 mm, 13 km from the observed storm (distance between recorded and simulated maximum accumulated rain). The storm trajectory is comparable with the radar data (Fig. 13g). Therefore, the simulation with the most realistic orography reproduces the storm evolution more realistically (Table 2, TDSM and MSD values).

6. Sensitivity to the Sea Surface Temperature

On July 9–10, 2019, an SST anomaly close to +4.4 °C was detected in the central Adriatic Sea (Fig. 3a). After the storm event, a decrease of the SST anomaly by 1.1 °C was observed (Fig. 3b) in the same area, probably caused by the oceanic wave breaking responsible for vertically mixing a large part of the heat in the mixed layer (Benetazzo et al., 2012). The mean maximum SST anomaly at the Adriatic basin scale reaches 2.7 °C before and 1.8 °C after the storm. As shown in Fig. 3a-b, strong anomaly values and a complex SST structure and evolution characterize the Adriatic Basin during the event. Based on this consideration, the impact of the SST on this event is investigated by using high-resolution SST datasets: the simulation CMEMS_TOPO is performed using the SST reanalysis dataset at 4.5-km resolution derived from the Copernicus Monitoring Environment Marine Service (Clementi et al., 2017; Pinardi et al., 2003), and the simulation SST_HR_1km_TOPO using the observed SST at 1-km resolution derived from the Copernicus CNR-GOS group datasets (Nardelli, 2012). In both simulations, the enhanced topography is implemented, considering its greater skill in reproducing the rainfall amount and distribution. Therefore, in the following discussion, the TOPOENHANC experiment is taken as a reference to evaluate the SST impact only. Therefore, a comparison between CMEMS_TOPO and TOPOENHANC is presented first, and then the comparison between SST_HR_1km_TOPO and TOPOENHANC.
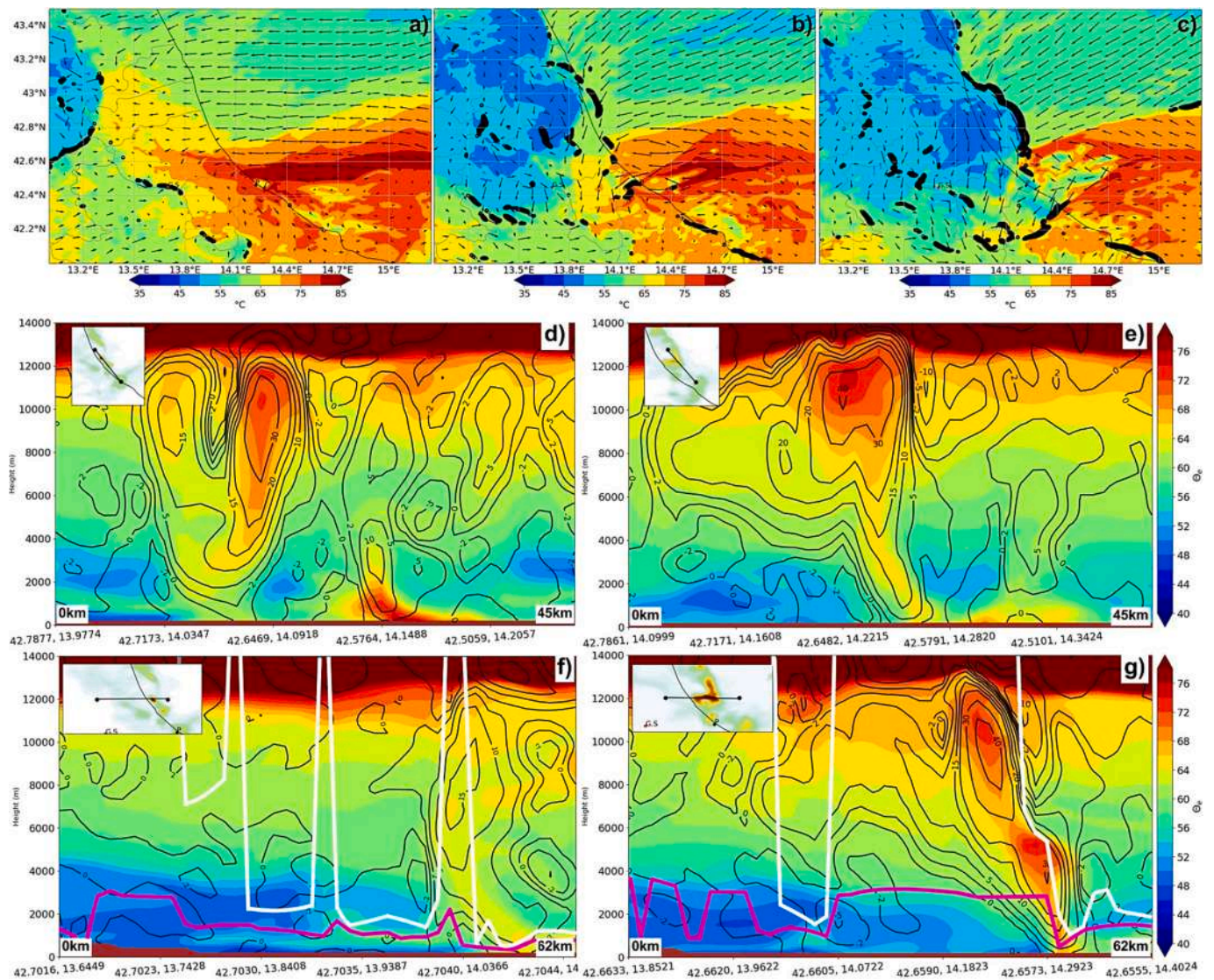
Fig. 14. TOPOENHANC Cold pool and frontal zone propagation at 8:30 (panel a), 9:40 (panel b), 10:10 (panel c). Panels d-g show the distribution of θe (°C, colour), vertical velocities (ms^{-1}, contours black lines), LFC in meters (white contours) and LCL in meters (magenta) along the two transects highlighted in the image, at 10:10 UTC (panel d-f) and 10:30 UTC (e-g). (For interpretation of the references to colour in this figure legend, the reader is referred to the web version of this article.)

6.1. TOPOENHANC versus CMEMS_TOPO

In order to investigate the impact of the CMEMS SST, the simulations CMEMS_TOPO and TOPOENHANC are compared in terms of the pointwise mean difference between TOPOENHANC and CMEMS_TOPO for SST, wind speed and heat fluxes at the time of maximum development of the storm cell (Fig. 15 a-c). Similarly, the differences of the two simulations for rainfall (Fig. 15e-h), hail (Fig. 15 f-i) and the front position (1000 hPa potential temperature in Fig. 15 d-g, black lines) are shown. As already known, higher SST values can lead to an intensification of wind speed, even at scales of a few tens of kilometers (Chelton, 2005; Ricchi et al., n.d.; Meroni et al., 2018; O'Neill et al., 2003, 2005, 2010) together with an increase of the heat fluxes. Fig. 15a shows a lower mean SST over the Adriatic Sea for CMEMS than for the ECMWF SST by approximately 0.7 °C. Conversely, near the area of the storm along the coast, the SST differences are negative suggesting a CMEMS SST greater than for the ECMWF SST by even 2.8–3 °C (Fig. 15a); therefore, a wind increase of up to 4 ms^{-1}, and a net heat flux increase of about 250 Wm^{-2} over this area occurs in the CMEMS_TOPO (Fig. 15 b-c). In this scenario, the cold pool (AM1) moves faster than AM3 close to the coast. Concerning the MAR (maximum accumulated rainfall),

CMEMS_TOPO shows on average better results (Table 2); also 145 mm/3 h is produced 15 km (maximum storm distance, MSD) away from the observed peak and the MHA (maximum hail accumulated) is 10 mm/3 h (Fig. 15 h-i).

6.2. Topography enhanced versus GOS 1 km HR SST

To compare the effect of the ECMWF SST and GOS SST (at 1-km resolution), the differences between TOPOENHANC (SST ECMWF-IFS) and SST_HR_1km_TOPO (SST GOS 1-km resolution) are shown in Fig. 16. A few studies (Ricchi et al., 2016, Carniel et al., 2016) showed an overestimation of the SST in ECMWF-IFS dataset, specifically over the semi-enclosed north Adriatic basin. In fact, at basin scale, the mean difference for SST between TOPOENHANC and SST_HR_1km_TOPO (Fig. 16a) is approximately 1.2 °C suggesting that the SST from ECMWF is warmer than the SST from GOS satellite. Conversely, as in the previous comparison (ECMWF SST – CMEMS SST), along the Marche-Abruzzo coastal area and along some isolated Croatian areas the differences are negative (SST anomaly 3–4 °C; Fig. 16a), suggesting GOS SST to be warmer than ECMWF SST. As previously discussed, these are the two areas with strong anomalies of SST during these days. The ability of the
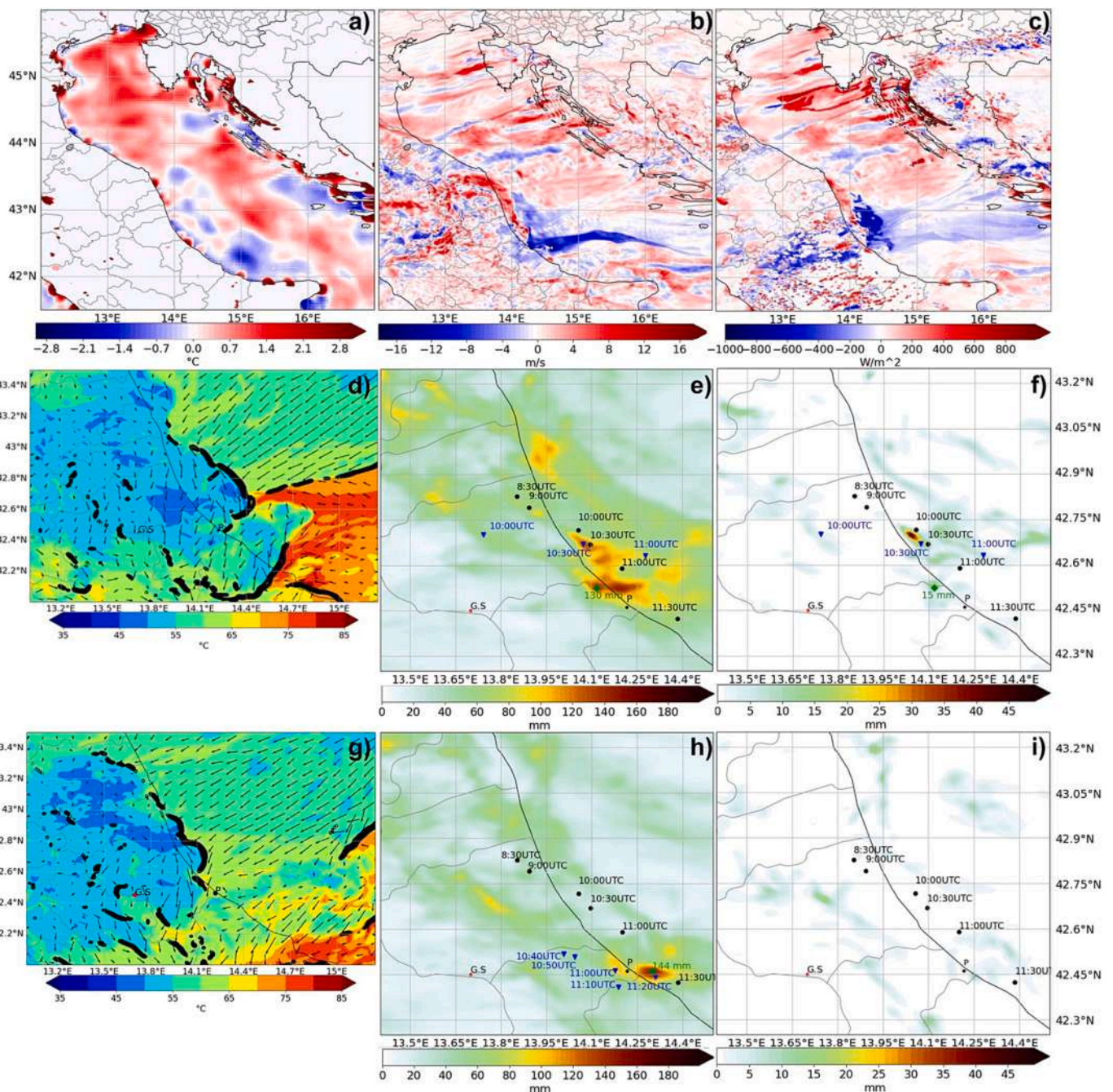
Fig. 15. Panels a-c show the difference (at 9:10UTC) between the ECMWF-IFS SST (TOPOENHANC) and CMEMS SST in term of SST, wind speed and heat fluxes. Panels d-f show the storm line, 3-h accumulated rain and hail for TOPOENHANC. Panels g-i for CMEMS_TOPO.

satellite dataset to discriminate their intensity supports the better quality of this data (Marullo et al., 2014, Nardelli et al., 2013; Ricchi et al. 2016; Carniel et al., 2016, Cassola et al., 2016). At the same time, the mean wind speed differences, at basin scale is 1.5–2 ms^{-1} (Fig. 16b), suggesting that the TOPOENHANC wind is larger than that in SST_HR_1km_TOPO. The same result is obtained for the net heat fluxes: TOPOENHANC heat fluxes are greater than those in SST_HR_1km_TOPO up to 260 Wm^{-2}, with a peak of 300 Wm^{-2} over the northern Adriatic Sea (Fig. 16c). Similar differences are also found in the southern Adriatic (Fig. 16a-c). The different SST in the two simulations has an impact on both the location and the intensity of the precipitation. For SST_HR_1km_TOPO, the maximum accumulated precipitation is 127 mm and the maximum hailfall is 10–12 mm/3 h (Fig. 16 h, i). Thus, the SST GOS HR 1 km can correctly reproduce the timing of the storm as

well as its path along the coast, although it underestimates the hailfall. The MSD (mean storm distance) between the SST_HR_1km_TOPO cell and the radar one is close to 10 km (Table 2), and the distance between the SST_HR_1km_TOPO maximum accumulated precipitation and the observed is approximately 10 km. The SST_HR_1km_TOPO highlights the peculiar dynamics, already observed in other very intense supercells (Gentile et al., 2014). In summary, the SST_HR_1km_TOPO shows a more realistic representation of the storm in space and time than the others: it reproduces the storm with only 20 min of delay.

6.3. Sensitivity to SST anomaly

To investigate the impact of the SST anomaly a simulation (SSTNOANM) was performed removing the SST anomaly.
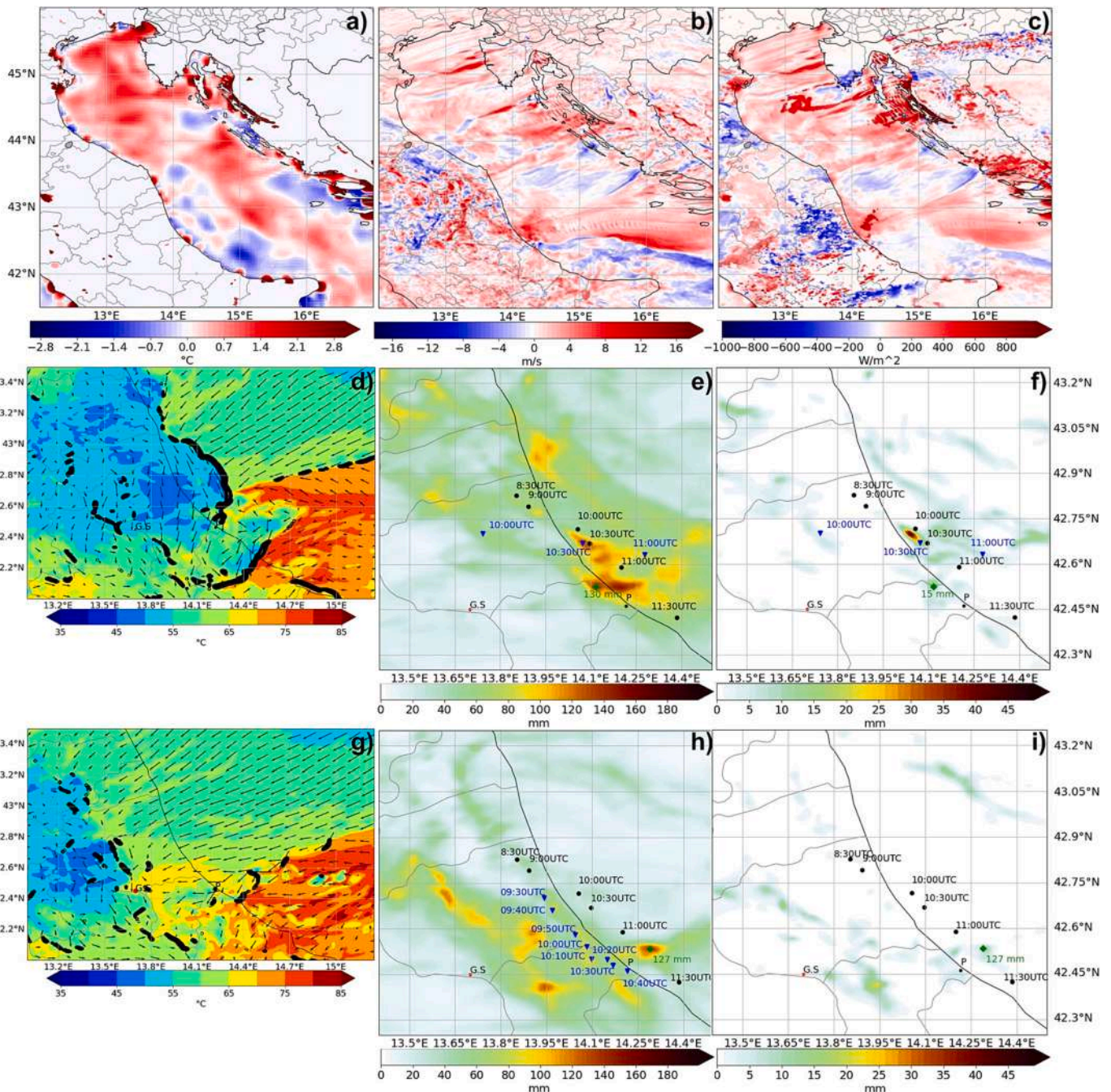
Fig. 16. Panels a-c show the difference, before the storm explosive intensification over Pescara, between ECMWF-IFS SST (TOPOENHANC) and SST_HR_1km_TOPO in terms of SST, wind speed, and surface heat fluxes. In panels d-f and g-i the frontal area and air masses, the accumulated rain, and accumulated hail, respectively for TOPOENHANC and SST_HR_1km_TOPO runs, are shown.

The SSTNOANM experiment aims to investigate the impact of the SST anomaly on the atmospheric dynamics and hailstorm structure. In this study we investigate the impact of the SST anomaly at the Adriatic basin scale; the importance of the latter scale is suggested by a number of factors from the control simulation, such as

1. The Bora wind over the Adriatic sea flows from the Croatian coast, where the air mass is very dry, to the Italian coast, where it has partially acquired heat and moisture from the sea.
2. The hailstorm develops downstream near the Italian coast of the Adriatic Sea, after strong air-sea interactions.
3. The relevant SST anomaly effect on heat fluxes is high.

Results characterizing the two runs and their differences are shown in Fig. 17 and Fig. 18. In order to simplify the interpretation, some variables are shown as differences between SST_HR_1km_TOPO SSTNOANM, others, are shown individually. Some variables are investigated only in this analysis, this is because they are more impacted and representative of air-sea interactions. Such as the Planetary Boundary Layer (PBL) height, that is strongly correlated with SST increases (as shown in Seo et al., 2014; Seo et al., 2007; Chelton, 2005; O'Neill et al., 2005).

The difference in SST between the two runs (SST observed and SST anomaly removed) is shown in (Fig. 17a, b): the difference has a peak of about 4.5 °C near the Abruzzo coast, over the basin where the storm intensifies rapidly. At the basin scale, the difference in SST is more
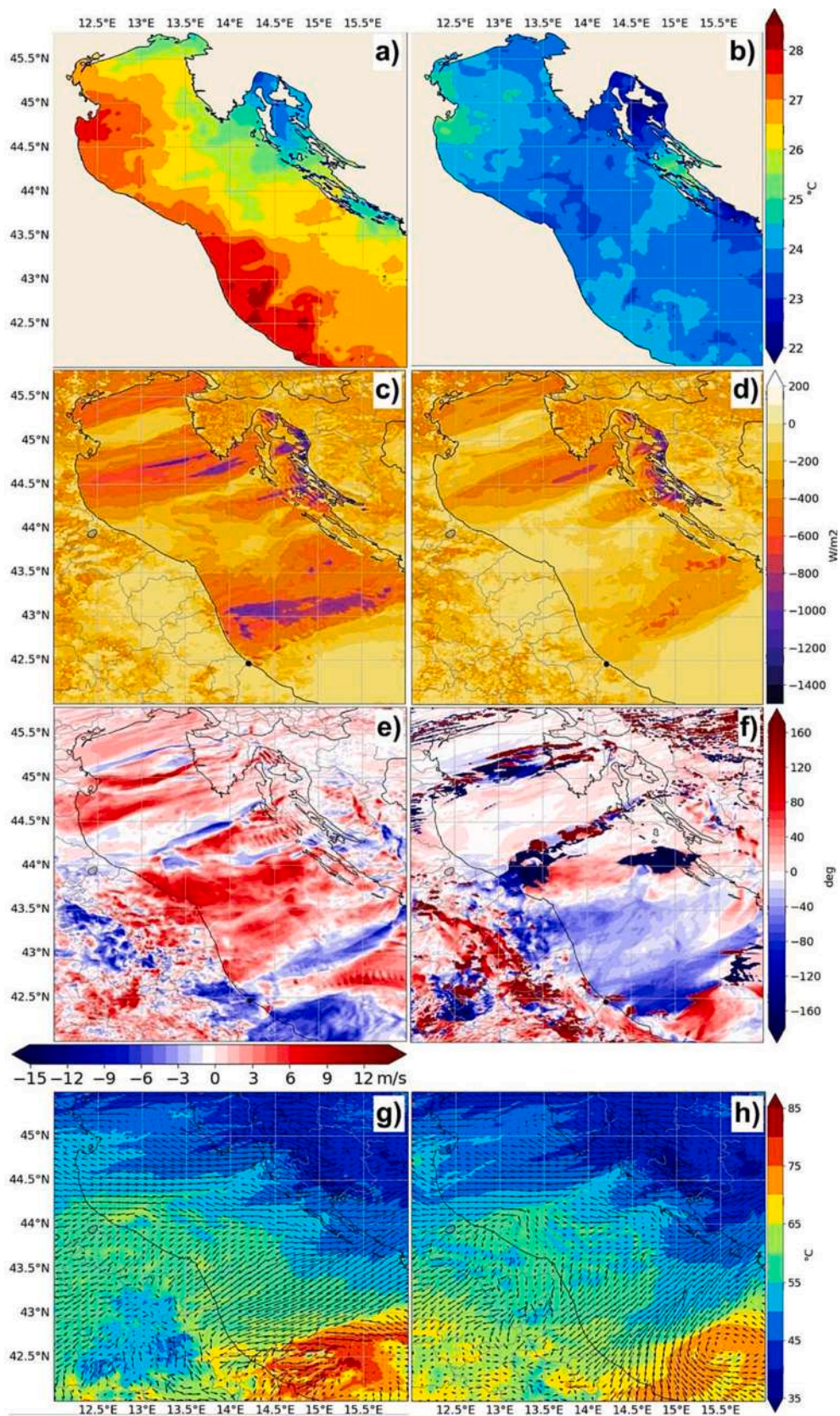
Fig. 17. Refers to the time 10:20 UTC and shows a,b) Sea Surface Temperature (°C), c,d) latent heat fluxes (Wm^{-2}), respectively for SST_HR_1km_TOPO and SSTNOANM. Panel e,f) show differences in wind speed (ms^{-1}) and wind direction (deg) between SST_HR_1km_TOPO and SSTNOANM runs, and g,h) show θe (°C) also for SST_HR_1km_TOPO run and SSTNOANM.
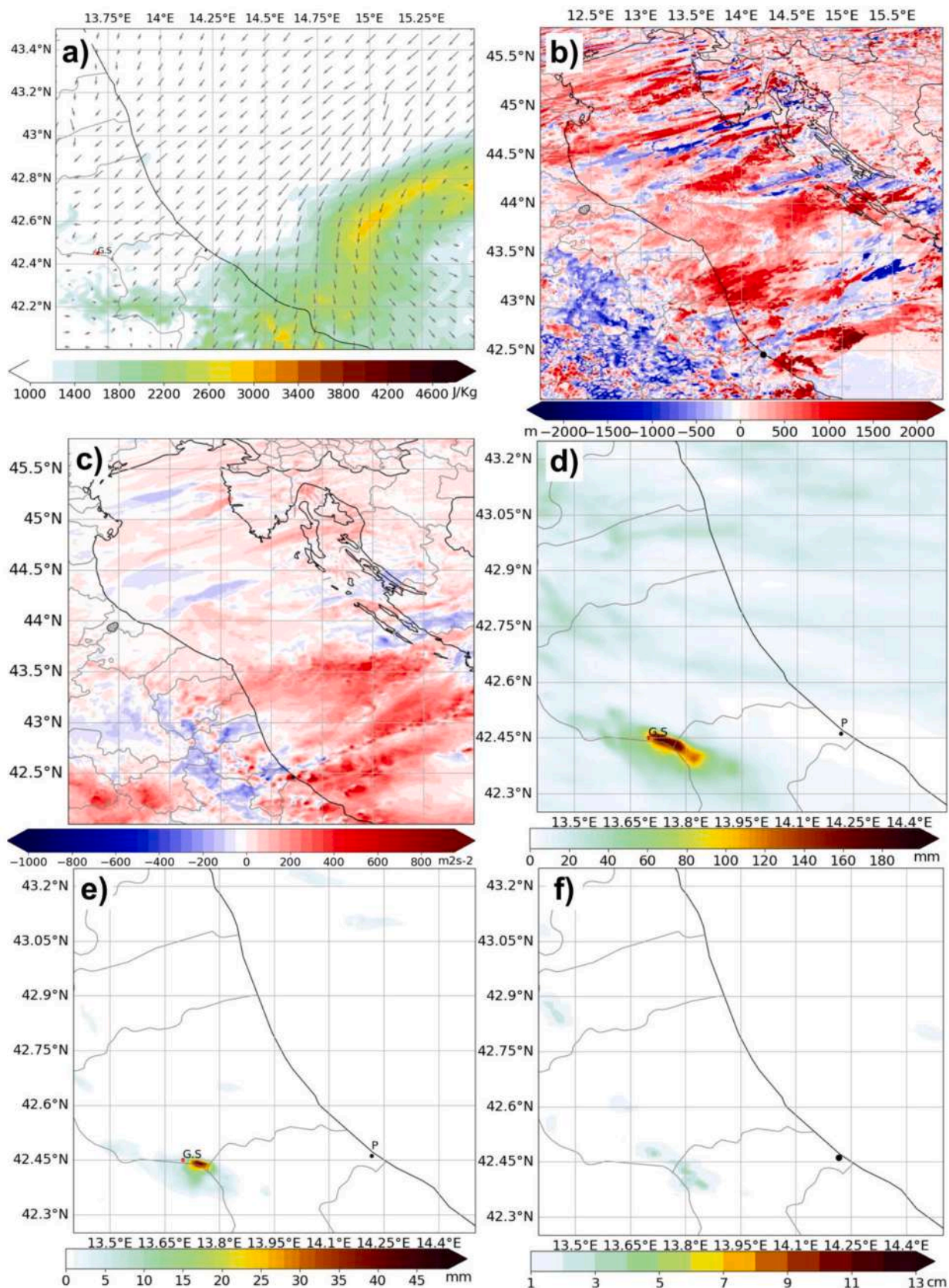
Fig. 18. Shows in panel a) CAPE index (Jkg^{-1}) for SSTNOANM run, b) PBL height (m) differences between SST_HR_1km_TOPO and SSTNOANM runs. Panel c) shows helicity (m^{2}s^{-2}) differences between SST_HR_1km_TOPO and SSTNOANM runs. Panel d) represent total rain accumulated (mm) in SSTMOD simulation, e) total hail accumulated (mm), and panel f) maximum hail diameter (cm) contained in atmosphere, calculated by HAILCAST module.

pronounced over the western sector of the Adriatic basin, compared with the eastern basin.

As shown in Fig. 17c, the SST_HR_1km_TOPO run displays Latent Heat (LH) fluxes, greater than 1400 Wm^{-2} near the Croatian coast, where temperature and vapor differences are greatest.

In AM1, LH reaches a maximum value of 1200 Wm^{-2} in the northern Bora jet (hereafter abbreviated as NBJ) and 1100 Wm^{-2} in the Bora Jet in the Event area (BJE), with an average LH of about 450 Wm^{-2} during the maximum development phase of the storm.

In AM2, LH is about −100 Wm^{-2} (from atmosphere to sea) during the development of the event, though it reaches −200 Wm^{-2} earlier (not shown).

Conversely, in SSTNOANM (Fig. 17d), in AM1, LH reaches about 800 Wm^{-2} in the NBJ, 450 Wm^{-2} in the BJE, and has a mean value of 280 Wm^{-2} over the north-central Adriatic basin.

Maximum net heat fluxes in AM1, for SST_HR_1km_TOPO run, are 1300 Wm^{-2} in NBJ, 1600 Wm^{-2} in the BJE, with a mean value of 550 Wm^{-2}. In SSTNOANM, maximum values of 800 Wm^{-2} are observed in the NBJ of AM1 and about 600 Wm^{-2} in some areas of the BJE and 450 Wm^{-2} on average. In AM2, SSTNOANM shows negative net heat fluxes (from the atmosphere to the sea) exceeding −300 Wm^{-2}. As shown in Fig. 17e the SST_HR_1km_TOPO shows higher wind intensities of about 5 ms^{-1} on average at the basin scale, 8–10 ms^{-1} in the NBJ, with peaks of 10–12 ms^{-1} in the BJE and the central area of the Adriatic basin, where the differences in SST are greatest. Some negative values are evident along the edges of the bora jets. This is due to the more intense and channeled (narrow) structure of the bora jets in SST_HR_1km_TOPO, compared to SSTNOANM (Fig. 17e,f). SST_HR_1km_TOPO shows a more intense structured cyclonic circulation, compared to SSTNOANM, causing more intense winds of about 12–14 ms^{-1}. The wind (Fig. 17f) shows a rotation of about −40/−60 deg. in the air of south-central AM1, while a positive rotation is observed, of about 35–45 deg. around 44°N and 15 deg. in mean in NBJ area. A stronger rotation, with positive values of about 70 deg., is observed in the cyclonic structure of AM2. The described dynamics affect the characteristic of the air mass. As shown in Fig. 17g,h, SST_HR_1km_TOPO shows higher θe values of about 60–65 °C in the central zone of AM1, 45–50 °C in the NBJ. AM2 is characterized by moist, milder air masses (not shown) with θe values between 80 and 85 °C. Conversely, in SSTNOANM, values of 50 °C in the central zone, 40–45 °C in the NBJ and 65–70 °C in AM2 are observed. In general, SSTNOANM shows air masses with θe values between 5 and 15 °C colder, than in SST_HR_1km_TOPO, with particular prominence in AM2. As shown in Fig. 18a, b by removing the SST anomaly, the CAPE index values show significant differences from SST_HR_1km_TOPO in AM2, respectively a maximum of 2800 Jkg^{-1} in SSTNOANM (Fig. 18a) and values greater than 4500 Jkg^{-1} in SST_HR_1km_TOPO (Figure Suppl_3). The PBL heights, Fig. 18b, are important for understanding the impact of air-sea interactions on the lower atmosphere and the lower level jet. AM1 shows PBL height differences between the two experiments, reaching about 2000 m with higher value in SST_HR_1km_TOPO run near the frontal zone (around AM1 and AM2), where air-sea interactions are most intense, as shown in Fig. 17 c,f. In terms of helicity, the differences between SST_HR_1km_TOPO and SSTNOANM, as shown in Fig. 18c, reach a peak of 800 m^{2}s^{-2} in the storm area, so that there is presumably a supercell development in SST_HR_1km_TOPO. Also, over the area AM2 and broadly in BJE area, there are differences of up to 500 m^{2}s^{-2} in terms of helicity. The accumulated precipitation and hail (Fig. 18d,e) in SSTNOANM show a MAR value of 165 mm, TDMS of −20 min, MHA of 47 mm, and MSD of 35 km, and are localized inland, near the Gran Sasso Masiff. Fig. 18f and Figure Suppl_3 show the hail size estimated with the HAILCAST module, about 2–4 cm in SSTNOANM, and 7 cm in SST_HR_1km_TOPO, respectively.

7. Discussion and conclusions

Time and space predictability of destructive weather extremes characterized by intense convective phenomena, such as supercells, is still challenging. Often, the physical mechanisms driving the dynamics and thermodynamics of the phenomena are not adequately represented in numerical wearther prediction models. Starting from this assumption, the mechanisms underlying the formation and intensification of the storm formed along the coast of the Abruzzo Italian region, in the central Adriatic Sea, on 10 July 2019 is investigated in this study (Montopoli et al., 2021; Tiesi et al., 2022). The storm moved along the coast and produced intense winds, precipitation of approximately 127 mm, and hail approximately 14 cm in size, around area of study. Deep convective cells moving along the coast are often observed in this area, but it is extremely rare to observe such intense phenomena. To investigate the mechanisms for triggering and sustaining the cell, the WRF numerical model with a convection-permitting approach is used to investigate the sensitivity to both the topography and the SST field. Moreover, the HAILCAST module is used for all the experiments to estimate the hail maximum dimension in the vertical column.

Starting from the control configuration, obtained after sensitivity studies, appropriately tuned for this event, several experiments are performed with the aim of investigating the role of the topography and of the SST. Concerning the topography, the following numerical simulations are performed:

- Two experiments removing the mountain ranges of the Sibillini Mountains first and then both Sibillini and Gran Sasso mountain;
- An experiment where the model topography of the main mountain ranges is corrected by filling the gap with the "true" elevation (e.g., 400–500 m are added to the highest peaks of the Gran Sasso and Sibillini mountains).

Based on the results of these experiments, the best configuration (the one with the corrected topography) is used for exploring the sensitivity to a few different SST datasets. The experiments are performed using:

- The default SST of the ECMWF-IFS model (9-km resolution);
- The SST taken from the dataset of the CMEMS Copernicus operational ocean model, at 4.5-km resolution;
- The SST from the GOS-Copernicus dataset at 1-km resolution;
- The SST from the GOS-Copernicus dataset at 1-km resolution with SST anomaly removed.

In general, the results show that the cell develops downwind of the Apennine chain, from the interaction of three air masses. As represented in Fig. 19, one from the northeast, dry and relatively cold (AM1), another one coming from the southeast over the Adriatic basin, warm and humid (AM2), and the third one associated to the minimum surface pressure over central and southern Italy, which is dry and relatively cold (AM3) coming from west. This airflow can be represented in two parts, the lower part (925 hPa), which remains trapped by the Apennines, particularly by the massifs of the Sibillini Mountains and Gran Sasso, and the second, which flows above these mountain ranges. The latter airmass is guided by the topography and by the interaction with the air masses coming from east (AM1 and AM2). The numerical experiments highlight the role of the topography by showing that if the highest peaks are not correctly represented, the densest part of AM3 overflows and reaches the coast, pushing the cell into the open sea, dramatically modifying the dynamics of the phenomenon.

Based on the results of the first set of experiments highlighting the physical mechanisms that trigger and drive the evolution of the storm, the following can be stated concerning the topography:

1. The high mountain peaks strongly influence the position of the storm cell, and its evolution downwind. As the results show, and as
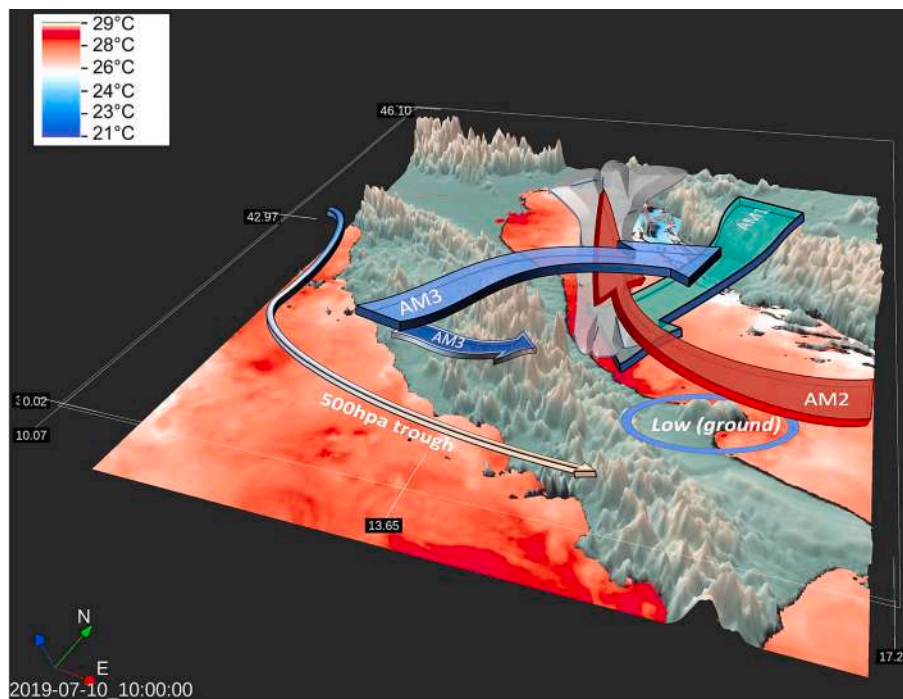
Fig. 19. Schematic structure of domain d02 orography and SST (using Vapor Gui Li et al., 2019, https://ncar.github.io/VaporDocumentationWebsite/citationAndLicense.html), and airmasses, AM1 in light green (925 hPa), AM2 (925 hPa) in light red, upper-level flow of AM3 (500 hPa) in light blue, lower level AM3, blocked by topography, in blue (925 hPa), and 500 hPa trough that develop along the Tyrrhenian Coast. (For interpretation of the references to colour in this figure legend, the reader is referred to the web version of this article.)

depicted in Fig. 19, if the topography is better represented in the model, the Monti Sibillini and Gran Sasso act as a barrier blocking the cold and dry air mass from arriving from inland. The lower layer cold pool is correctly blocked for many hours, whereas its most unstable part is forced eastward and pushed upward flowing over AM1 and AM2. The interaction of these latter air masses produces intense wind shear (Figure Suppl_2) and strong vertical temperature and humidity gradients. Hence, the improved representation of the topography impacts the location, intensity, dynamics, and morphology of the storm cell;

2. If the topography is underestimated, the blocking effect is missed and an acceleration of the cold pool along the slope of the mountains is produced. This results in the interaction of the three air masses in the wrong place and time, drastically changing the representation of the phenomenon. Indeed, if the speed and density of the cold pool are larger than the real ones, a more intense interaction with the humid air mass over the sea occurs, feeding the convective system which incorrectly moves to the open sea, away from the coast; if these peaks are removed, the convergence of the air masses occurs tens of kilometers inland, suggesting that the phenomenon is not driven only by the synoptic scale, but that the local scale plays a key role.

Concerning the impact of the SST, the following can be stated:

1. The SST drives the development of the storm along the coast (in the supplementary material the evolution of the cell is shown for each simulation);
2. If the CMEMS SST (with a comparable resolution to ECMWF SST) is used, the storm dynamics slightly change by making the cold pool (AM1) move faster than the air coming from the Apennines (AM3) and constraining AM3 to be close to the coast. No large variation in timing and location of the storm cell is found, in general only of a few tens of minutes.
3. If the 1-km GOS SST is used, the storm timing and displacement are correctly represented, with a structure parallel to the coast and

moving along the coast from north to south. Moreover, this experiment correctly reproduces the interaction of the two cells, transforming them into a double updraft supercell in its mature phase.

4. The key role played by the SST field, in particular its anomaly, on the formation of this event was demonstrated. In fact, by removing the SST anomaly, the heat fluxes decrease drastically (particularly in AM1); this results in a slower wind speed, a clockwise rotation in the southern part of AM1 and a counterclockwise in the northern part, consistent with the SST gradients traversed by the wind. These dynamics transfer less heat and moisture to the air, which consequently obtains lower θe values, lower CAPE by about 40–45%, a consistent decrease in PBL height, and a drastic decrease in helicity in the storm area. Consequently, the precipitation shows a different structure with respect to the run that implements the SST anomaly. The precipitation is weaker, spatially shifted and localized closer to the Apennines, and occurs in several individual events, and not in one single and intense storm. In addition, a strong decrease in the size of hailstone contained in the air column is observed.

The initial question on the ability of WRF at a grid spacing of 1 km to faithfully reproduce the structure and characteristics of a system characterized by a strong hailstorm, with hailstones of extreme size (especially for these areas), is largely addressed: the results show that WRF can reproduce not only the dynamics and thermodynamics of the storm, but also the observed cell well localized in space and time. Moreover, it can reproduce the accumulated rain and the hail size. This comes after extensive tuning to get the best configuration for this study area and this event.

In conclusion, the results of this study suggest that this phenomenon is strongly linked to and guided by the dynamics on a local scale and the topography plays a key role as well as the SST and, in particular its anomaly. We also point out the relevance of a proper numerical setup necessary to reproduce the event, among others: many vertical levels, with the first level very close to the ground for correctly reproducing the air-sea interactions; a high-frequency output (10 min) to capture the

dynamics and thermodynamics of the phenomenon, a microphysics scheme implementing numerous classes of hydrometeors, like graupel and hail, an adequate timestep to resolve the dynamics of this phenomenon and other physical and dynamic settings, which can influence the quality of simulations of such complex and intense events. Subsequently, it might be may be difficult to generalize results belonging to experiment configurarations presented in this study since providing indications specific for this event. We advocate that numerous tests be conducted in order to implement the configuration that best represents the event on a case-by-case basis.

Nevethless, these findings are important not only from the scientific point of view, but also for weather forecasting in a fast-changing climate, where exacerbated SST anomalies supply a surplus of energy to extremes triggering and development. It is indeed essential to implement forecasting systems capable to catch the right energy anomalies of the system, through an adequate high resolution and physics settings.

Finally, further analyses are needed to investigate if the intensity and the structure of the storm correspond to a supercell and if the model can reproduce the distribution and the amount of the hydrometeors comparably to the numerical work by the companion paper Ricchi et al., n.d., Tiesi et al. (2022) and the observation by Montopoli et al. (2021).

CRediT authorship contribution statement

Antonio Ricchi: Conceptualization, Investigation, Methodology, Data curation, Formal analysis, Writing – original draft, Writing – review & editing. **Lorenzo Sangelantoni:** Writing – original draft, Writing – review & editing. **Gianluca Redaelli:** Writing – original draft, Writing – review & editing. **Vincenzo Mazzarella:** Writing – original draft, Writing – review & editing. **Mario Montopoli:** Data curation, Writing – original draft, Writing – review & editing. **Mario Marcello Miglietta:** Investigation, Writing - original draft, Writing - review & editing. **Alessandro Tiesi:** Writing – original draft, Data curation. **Simone Mazzà:** Data curation. **Richard Rotunno:** Visualization, Investigation, Supervision, Writing – original draft, Writing – review & editing. **Rossella Ferretti:** Funding acquisition, Conceptualization, Supervision, Writing - original draft, Writing - review & editing.

Declaration of Competing Interest

The authors declare that the research was conducted in the absence of any commercial or financial relationships that could be construed as a potential conflict of interest.

Data availability

Data will be made available on request.

Acknowledgments

Appendix A. Supplementary data

Supplementary data to this article can be found online at https://doi.org/10.1016/j.atmosres.2023.107078.

References

Abrams, M., Crippen, R., Fujisada, H., 2020. ASTER global digital elevation model (GDEM) and ASTER global water body dataset (ASTWBD). Remote Sens. 12 (7), 1156. https://doi.org/10.3390/RS12071156.

Antonescu, B., Schultz, D.M., Holzer, A., Groenemeijer, P., 2017. Tornadoes in Europe: an Underestimated Threat. Bull. Am. Meteorol. Soc. 98 (4), 713–728. https://doi.org/10.1175/BAMS-D-16-0171.1.

Avolio, E., Miglietta, M.M., 2023. A Comparative analysis of two mediterranean tornado hotspots. Atmosphere 14 (1), 189. https://doi.org/10.3390/ATMOS14010189.

Bagaglini, L., Ingrosso, R., Miglietta, M.M., 2021. Synoptic patterns and mesoscale precursors of Italian tornadoes. Atmos. Res. 253, 105503 https://doi.org/10.1016/J.ATMOSRES.2021.105503.

Barthlott, C., Davolio, S., 2016. Mechanisms initiating heavy precipitation over Italy during HyMeX special Observation Period 1: a numerical case study using two mesoscale models. Q. J. R. Meteorol. Soc. 142 (1), 238–258. https://doi.org/10.1002/QJ.2630.

Belušić, D., Žagar, M., Grisogono, B., 2007. Numerical simulation of pulsations in the bora wind. Q. J. R. Meteorol. Soc. 133 (627), 1371–1388. https://doi.org/10.1002/QJ.129.

Belušić, D., Hrastinski, M., Vežcenaj, Z., Grisogono, B., 2013. Wind regimes associated with a mountain gap at the Northeastern Adriatic Coast. J. Appl. Meteorol. Climatol. 52 (9), 2089–2105. https://doi.org/10.1175/JAMC-D-12-0306.1.

Benetazzo, A., Fedele, F., Carniel, S., Ricchi, A., Bucchignani, E., Sclavo, M., 2012. Wave climate of the Adriatic Sea: a future scenario simulation. Nat. Hazards Earth Syst. Sci. 12 (6), 2065–2076. https://doi.org/10.5194/NHESS-12-2065-2012.

Bentamy, A., Grodsky, S.A., Carton, J.A., Croizé-Fillon, D., Chapron, B., 2012. Matching ASCAT and QuikSCAT winds. J. Geophys. Res. Oceans 117 (C2), 2011. https://doi.org/10.1029/2011JC007479.

Bergamasco, A., Gačić, M., 1996. Baroclinic response of the Adriatic Sea to an episode of Bora Wind. J. Phys. Oceanogr. 26 (7), 1354–1369. https://doi.org/10.1175/1520-0485(1996)026.

Blumen, W., 1992. Propagation of fronts and frontogenesis versus frontolysis over orography. Meteorog. Atmos. Phys. 48 (1–4), 37–50. https://doi.org/10.1007/BF01029558/METRICS.

Brimelow, J.C., Reuter, G.W., 2009. Explicit forecasts of hail occurrence and expected hail size using the GEM-HAILCAST system with a rainfall filter. Weather Forecast. 24 (4), 935–945. https://doi.org/10.1175/2009WAF2222138.1.

Capozzi, V., Annella, C., Budillon, G., 2023. Classification of daily heavy precipitation patterns and associated synoptic types in the Campania Region (southern Italy). Atmos. Res. 289, 106781. https://doi.org/10.1016/J.ATMOSRES.2023.106781.

Carniel, S., Benetazzo, A., Bonaldo, D., Falcieri, F.M., Miglietta, M.M., Ricchi, A., Sclavo, M., 2016. Scratching beneath the surface while coupling atmosphere, ocean and waves: analysis of a dense water formation event. Ocean Model 101, 101–112. https://doi.org/10.1016/J.OCEMOD.2016.03.007.

Cassola, F., Ferrari, F., Mazzino, A., Miglietta, M.M., 2016. The role of the sea on the flash floods events over Liguria (northwestern Italy). Geophys. Res. Lett. 43 (7), 3534–3542. https://doi.org/10.1002/2016GL068265.

Chelton, D.B., 2005. The impact of SST specification on ECMWF surface wind stress fields in the Eastern Tropical Pacific. J. Clim. 18 (4), 530–550. https://doi.org/10.1175/JCLI-3275.1.

Clementi, E., Oddo, P., Drudi, M., Pinardi, N., Korres, G., Grandi, A., 2017. Coupling hydrodynamic and wave models: first step and sensitivity experiments in the Mediterranean Sea. Ocean Dyn. 67 (10), 1293–1312. https://doi.org/10.1007/S10236-017-1087-7/TABLES/11.

Cushman-Roisin, B., Korotenko, K.A., Galos, C.E., Dietrich, D.E., 2007. Simulation and characterization of the Adriatic Sea mesoscale variability. J. Geophys. Res. Oceans 112 (C3), 3–14. https://doi.org/10.1029/2006JC003515.

Davies, H.C., Pichler, H., 1990. Mountain meteorology and ALPEX; an introduction. Meteorog. Atmos. Phys. 43, 3–4. https://doi.org/10.1007/BF01028104.

Davolio, S., Ferretti, R., Baldini, L., Casaioli, M., Cimini, D., Ferrario, M.E., Gentile, S., Loglisci, N., Maiello, I., Manzato, A., Mariani, S., Marsigli, C., Marzano, F.S., Miglietta, M.M., Montani, A., Panegrossi, G., Pasi, F., Pichelli, E., Pucillo, A., Zinzi, A., 2015a. The role of the Italian scientific community in the first HyMeX SOP: an outstanding multidisciplinary experience, 24 (3), 261–267. https://doi.org/10.1127/metz/2015/0624.

Davolio, S., Silvestro, F., Malguzzi, P., 2015b. Effects of increasing horizontal resolution in a convection-permitting model on flood forecasting: the 2011 dramatic events in Liguria, Italy. J. Hydrometeorol. 16 (4), 1843–1856. https://doi.org/10.1175/JHM-D-14-0094.1.

Davolio, S., Silvestro, F., Gastaldo, T., 2017. Impact of rainfall assimilation on high-resolution hydrometeorological forecasts over Liguria, Italy. J. Hydrometeorol. 18 (10), 2659–2680. https://doi.org/10.1175/JHM-D-17-0073.1.

Dotzek, N., Groenemeijer, P., Feuerstein, B., Holzer, A.M., 2009. Overview of ESSL's severe convective storms research using the European Severe Weather Database ESWD. Atmos. Res. 93 (1–3), 575–586. https://doi.org/10.1016/J.ATMOSRES.2008.10.020.

Ducrocq, V., Braud, I., Davolio, S., Ferretti, R., Flamant, C., Jansa, A., Kalthoff, N., Richard, E., Taupier-Letage, I., Ayral, P.A., Belamari, S., Berne, A., Borga, M., Boudevillain, B., Bock, O., Boichard, J.L., Bouin, M.N., Bousquet, O., Bouvier, C., Tamayo, J., 2014. HyMeX-SOP1: the field campaign dedicated to heavy precipitation and flash flooding in the Northwestern Mediterranean. Bull. Am. Meteorol. Soc. 95 (7), 1083–1100. https://doi.org/10.1175/BAMS-D-12-00244.1.

Dudhia, J., 1989. Numerical study of convection observed during the Winter Monsoon Experiment using a mesoscale two-dimensional model. J. Atmos. Sci. 46 (20) https://doi.org/10.1175/1520-0469(1989)046<3077:NSOCOD>2.0.CO;2.

Duffourg, F., Nuissier, O., Ducrocq, V., Flamant, C., Chazette, P., Delanoë, J., Doerenbecher, A., Fourrié, N., di Girolamo, P., Lac, C., Legain, D., Martinet, M., Saïd, F., Bock, O., 2016. Offshore deep convection initiation and maintenance during the HyMeX IOP 16a heavy precipitation event. Q. J. R. Meteorol. Soc. 142 (1), 259–274. https://doi.org/10.1002/QJ.2725.

Gentile, S., Ferretti, R., Marzano, F.S., 2014. Investigating Hector Convective Development and Microphysical Structure using High-Resolution Model Simulations, Ground-based Radar Data, and TRMM Satellite Data. J. Atmos. Sci. 71 (4), 1353–1370. https://doi.org/10.1175/JAS-D-13-0107.1.

Giaiotti, D., Nordio, S., Stel, F., 2003. The climatology of hail in the plain of Friuli Venezia Giulia. Atmos. Res. 67–68, 247–259. https://doi.org/10.1016/S0169-8095 (03)00084-X.

Grisogono, B., Belušić, D., 2009. A review of recent advances in understanding the meso- and microscale properties of the severe Bora wind. Tellus A 61 (1), 1–16. https://doi.org/10.1111/J.1600-0870.2008.00369.X.

Janjić, Z.I., Janjić, I.Z., 1994. The step-mountain eta coordinate model: further developments of the convection, viscous sublayer, and turbulence closure schemes. MWRv 122 (5), 927. https://doi.org/10.1175/1520-0493(1994)122.

Khodayar, S., Davolio, S., di Girolamo, P., Lebeaupin Brossier, C., Flaounas, E., Fourrie, N., Lee, K.O., Ricard, D., Vie, B., Bouttier, F., Caldas-Alvarez, A., Ducrocq, V., 2021. Overview towards improved understanding of the mechanisms leading to heavy precipitation in the western Mediterranean: Lessons learned from HyMeX. Atmos. Chem. Phys. 21 (22), 17051–17078. https://doi.org/10.5194/ACP-21-17051-2021.

Lee, K.O., Flamant, C., Ducrocq, V., Duffourg, F., Fourrié, N., Delanoë, J., Bech, J., 2017. Initiation and development of a mesoscale convective system in the Ebro River Valley and related heavy precipitation over northeastern Spain during HyMeX IOP 15a. Q. J. R. Meteorol. Soc. 143 (703), 942–956. https://doi.org/10.1002/QJ.2978.

Li, S., Jaroszynski, S., Pearse, S., Orf, L., Clyne, J., 2019. VAPOR: a visualization package tailored to analyze simulation data in Earth system science. Atmosphere. 10 (9), 488. https://doi.org/10.3390/atmos10090488.

Lionello, P., Abrantes, F., Congedi, L., Dulac, F., Gačić, M., Gomis, D., Goodess, C., Hoff, H., Kutiel, H., Luterbacher, J., Planton, S., Reale, M., Schröder, K., Vittoria Struglia, M., Toreti, A., Tsimplis, M., Ulbrich, U., Xoplaki, E., 2012. Introduction: Mediterranean Climate—Background Information. The Climate of the Mediterranean Region: From the Past to the Future, pp. xxxv–xc. https://doi.org/10.1016/B978-0-12-416042-2.00012-4.

Manzato, A., Davolio, S., Miglietta, M.M., Pucillo, A., Setvák, M., 2014. 2 September 2012: A Supercell Outbreak in NE Italy? https://doi.org/10.1016/j.atmosres.2014.07.019.

Marullo, S., Santoleri, R., Ciani, D., le Borgne, P., Péré, S., Pinardi, N., Tonani, M., Nardone, G., 2014. Combining model and geostationary satellite data to reconstruct hourly SST field over the Mediterranean Sea. Remote Sens. Environ. 146, 11–23. https://doi.org/10.1016/J.RSE.2013.11.001.

Mastrangelo, D., Horvath, K., Riccio, A., Miglietta, M.M., 2011. Mechanisms for convection development in a long-lasting heavy precipitation event over southeastern Italy. Atmos. Res. 100 (4), 586–602. https://doi.org/10.1016/J.ATMOSRES.2010.10.010.

Mazzarella, V., Maiello, I., Ferretti, R., Capozzi, V., Picciotti, E., Alberoni, P.P., Marzano, F.S., Budillon, G., 2020. Reflectivity and velocity radar data assimilation for two flash flood events in central Italy: A comparison between 3D and 4D variational methods. Q. J. R. Meteorol. Soc. 146 (726), 348–366. https://doi.org/10.1002/QJ.3679.

Meroni, A.N., Parodi, A., Pasquero, C., 2018. Role of SST patterns on Surface Wind Modulation of a Heavy Midlatitude Precipitation Event. J. Geophys. Res. Atmos. 123 (17), 9081–9096. https://doi.org/10.1029/2018JD028276.

Miglietta, M.M., Davolio, S., 2022. Dynamical forcings in heavy precipitation events over Italy: lessons from the HyMeX SOP1 campaign. Hydrol. Earth Syst. Sci. 26, 627–646. https://doi.org/10.5194/hess-26-627-2022.

Miglietta, M.M., Matsangouras, I.T., 2018. An updated "climatology" of tornadoes and waterspouts in Italy. Int. J. Climatol. 38 (9), 3667–3683. https://doi.org/10.1002/JOC.5526.

Miglietta, M.M., Manzato, A., Rotunno, R., 2016a. Characteristics and predictability of a supercell during HyMeX SOP1. Q. J. R. Meteorol. Soc. 142 (700), 2839–2853. https://doi.org/10.1002/QJ.2872.

Miglietta, M.M., Manzato, A., Rotunno, R., 2016b. Characteristics and predictability of a supercell during HyMeX SOP1. Q. J. R. Meteorol. Soc. 142 (700), 2839–2853. https://doi.org/10.1002/QJ.2872.

Miglietta, M.M., Mazon, J., Motola, V., Pasini, A., 2017a. Effect of a positive Sea Surface Temperature anomaly on a Mediterranean tornadic supercell. Sci. Rep. 7 (1), 1–8. https://doi.org/10.1038/s41598-017-13170-0.

Miglietta, M.M., Mazon, J., Rotunno, R., 2017b. Numerical simulations of a tornadic supercell over the Mediterranean. Weather Forecast. 32 (3), 1209–1226. https://doi.org/10.1175/WAF-D-16-0223.1.

Miglietta, M.M., Regano, A., 2008. Natural Hazards and Earth System Sciences An observational and numerical study of a flash-flood event over south-eastern Italy. Hazards Earth Syst. Sci. 8, 1417–1430.

Milbrandt, J.A., Yau, M.K., 2005. A multimoment bulk microphysics parameterization. Part I: analysis of the role of the spectral shape parameter. J. Atmos. Sci. 62 (9), 3051–3064. https://doi.org/10.1175/JAS3534.1.

Mlawer, E.J., Taubman, S.J., Brown, P.D., Iacono, M.J., Clough, S.A., 1997. Radiative transfer for inhomogeneous atmospheres: RRTM, a validated correlated-k model for the longwave. J. Geophys. Res. Atmos. 102 (D14), 16663–16682. https://doi.org/10.1029/97JD00237.

Montopoli, M., Picciotti, E., Baldini, L., di Fabio, S., Marzano, F.S., Vulpiani, G., 2021. Gazing inside a giant-hail-bearing Mediterranean supercell by dual-polarization Doppler weather radar. Atmos. Res. 264, 105852 https://doi.org/10.1016/J.ATMOSRES.2021.105852.

Morcrette, J.J., Boucher, O., Jones, L., Salmond, D., Bechtold, P., Beljaars, A., Benedetti, A., Bonet, A., Kaiser, J.W., Razinger, M., Schulz, M., Serrar, S., Simmons, A.J., Sofiev, M., Suttie, M., Tompkins, A.M., Untch, A., 2009. Aerosol analysis and forecast in the European Centre for medium-range weather forecasts integrated forecast system: forward modeling. J. Geophys. Res. Atmos. 114 (D6), 6206. https://doi.org/10.1029/2008JD011235.

Nardelli, B.B., 2012. A novel approach for the high-resolution interpolation of in situ sea surface salinity. J. Atmos. Ocean. Technol. 29 (6), 867–879. https://doi.org/10.1175/JTECH-D-11-00099.1.

Nardelli, B.B., Tronconi, C., Pisano, A., Santoleri, R., 2013. High and ultra-high resolution processing of satellite sea surface temperature data over southern European seas in the framework of MyOcean project. Remote Sens. Environ. 129, 1–16. In: https://www.academia.edu/26609056/High_and_Ultra_High_resolution_pr ocessing_of_satellite_Sea_Surface_Temperature_data_over_Southern_European_Seas_i n_the_framework_of_MyOcean_project. https://doi.org/10.1016/j.rse.2012.10.012.

Nuissier, O., Ducrocq, V., Ricard, D., Lebeaupin, C., Anquetin, S., 2008. A numerical study of three catastrophic precipitating events over southern France. I: Numerical framework and synoptic ingredients. Q. J. R. Meteorol. Soc. 134 (630), 111–130. https://doi.org/10.1002/QJ.200.

Nuissier, O., Joly, B., Joly, A., Ducrocq, V., Arbogast, P., 2011. A statistical downscaling to identify the large-scale circulation patterns associated with heavy precipitation events over southern France. Q. J. R. Meteorol. Soc. 137 (660), 1812–1827. https://doi.org/10.1002/QJ.866.

O'Neill, L.W., Chelton, D.B., Esbensen, S.K., 2003. Observations of SST-induced perturbations of the wind stress field over the Southern Ocean on seasonal timescales. J. Clim. 16 (14), 2340–2354. https://doi.org/10.1175/2780.1.

O'Neill, L.W., Chelton, D.B., Esbensen, S.K., Wentz, F.J., 2005. High-resolution satellite measurements of the atmospheric boundary layer response to SST variations along the Agulhas return current. J. Clim. 18 (14), 2706–2723. https://doi.org/10.1175/JCLI3415.1.

O'Neill, L.W., Chelton, D.B., Esbensen, S.K., 2010. The effects of SST-induced surface wind speed and direction gradients on midlatitude surface vorticity and divergence. J. Clim. 23 (2), 255–281. https://doi.org/10.1175/2009JCLI2613.1.

Parodi, A., Boni, G., Ferraris, L., Rudari, R., Siccardi, F., Parodi, A., Boni, G., Ferraris, L., Rudari, R., Siccardi, F., 2010. Hydro-meteorology research and ICT at CIMA foundation: DEWETRA and DRIHMS experiences. (Invited). AGUFM 2010. H53H-01. https://ui.adsabs.harvard.edu/abs/2010AGUFM.H53H..01P/abstract.

Pichelli, E., Rotunno, R., Ferretti, R., 2017. Effects of the Alps and Apennines on forecasts for Po Valley convection in two HyMeX cases. Q. J. R. Meteorol. Soc. 143 (707), 2420–2435. https://doi.org/10.1002/QJ.3096.

Pinardi, N., Allen, I., Demirov, E., de Mey, P., Korres, G., Lascaratos, A., le Traon, P.-Y., Maillard, C., Manzella, G., Tziavos, C., 2003. The Mediterranean Ocean Forecasting System: First Phase of Implementation (1998-2001), 21.

Pucillo, A., Miglietta, M.M., Lombardo, K., Manzato, A., 2020. Application of a simple analytical model to severe winds produced by a bow echo like storm in northeast Italy. Meteorol. Appl. 27 (1), e1868. https://doi.org/10.1002/MET.1868.

Punge, H.J., Bedka, K.M., Kunz, M., Reinbold, A., 2017. Hail frequency estimation across Europe based on a combination of overshooting top detections and the ERA-INTERIM reanalysis. Atmos. Res. 198, 34–43. https://doi.org/10.1016/J.ATMOSRES.2017.07.025.

Ricchi, A., Bonaldo, D., Cioni, G., Carniel, S., Miglietta, M.M., 2021.. Simulation of a flash-flood event over the Adriatic Sea with a high-resolution atmosphere-ocean-wave coupled system. https://doi.org/10.1038/s41598-021-88476-1.

Ricchi, A., Miglietta, M.M., Bonaldo, D., Cioni, G., Rizza, U., Carniel, S., 2019. Multi-physics ensemble versus Atmosphere–Ocean coupled model simulations for a tropical-like cyclone in the Mediterranean Sea. Atmosphere 10 (4), 202. https://doi.org/10.3390/ATMOS10040202.

Ricchi, A., Miglietta, M.M., Falco, P.P., Benetazzo, A., Bonaldo, D., Bergamasco, A., Sclavo, M., Carniel, S., 2016. On the use of a coupled ocean–atmosphere–wave model during an extreme cold air outbreak over the Adriatic Sea. Atmos. Res. 172–173, 48–65. https://doi.org/10.1016/J.ATMOSRES.2015.12.023.

Ricchi Antonio Rotunno; Miglietta Richard; Picciotti Mario Marcello; Montopoli Errico; Marzano Mario; Baldini Frank Silvio; Vulpiani Luca; Tiesi Gianfranco; Rossella Alessandro Ferretti, n.d.. Analysis of the Development Mechanisms of a Large-Hail Storm Event on the Adriatic Sea: Part II. (2015) 10.2139/ssrn.4535764. Available at SSRN https://ssrn.com/abstract=4535764.

Richard, E., Buzzi, A., Zängl, G., 2007. Quantitative precipitation forecasting in the Alps: the advances achieved by the Mesoscale Alpine Programme. Q. J. R. Meteorol. Soc. 133 (625), 831–846. https://doi.org/10.1002/qj.65.

Rotunno, R., Ferretti, R., 2001. Mechanisms of intense Alpine Rainfall. J. Atmos. Sci. 58 (13), 1732–1749. https://doi.org/10.1175/1520-0469(2001)058.

Rotunno, R., Houze, R.A., 2007. Lessons on orographic precipitation from the Mesoscale Alpine Programme. Q. J. R. Meteorol. Soc. 133 (625), 811–830. https://doi.org/10.1002/QJ.67.

Rotunno, R., Markowski, P.M., Bryan, G.H., 2017. "Near Ground" vertical vorticity in supercell thunderstorm models. J. Atmos. Sci. 74 (6), 1757–1766. https://doi.org/10.1175/JAS-D-16-0288.1.

Seo, H., Miller, A.J., Roads, J.O., 2007. The Scripps Coupled Ocean–Atmosphere Regional (SCOAR) model, with applications in the Eastern Pacific Sector. J. Clim. 20 (3), 381–402. https://doi.org/10.1175/JCLI4016.1.

Seo, H., Kwon, Y.-O., Park, J.-J., 2014. On the effect of the East/Japan Sea SST variability on the North Pacific atmospheric circulation in a regional climate model. J. Geophys. Res. Atmos. 119, 418–444. https://doi.org/10.1002/2013JD020523.

Shapiro, R., 1970. Smoothing, filtering, and boundary effects. Rev. Geophys. 8 (2), 359–387. https://doi.org/10.1029/RG008I002P00359.

Silvestri, L., Saraceni, M., Bongioannini Cerlini, P., 2022. Links between precipitation, circulation weather types and orography in central Italy. Int. J. Climatol. 42 (11), 5807–5825. https://doi.org/10.1002/JOC.7563.

Skamarock, W.C., Klemp, J.B., Dudhia, J., Gill, D.O., Barker, D.M., Duda, M.G., Huang, X.-Y., Wang, W., Powers, J.G., Skamarock, W.C., Klemp, J.B., Dudhia, J., Gill, D.O., Barker, D.M., Duda, M.G., Huang, X.-Y., Wang, W., Powers, J.G., 2008.

A description of the advanced research WRF version 3. NCATN 475, 1. https://doi.org/10.5065/D68S4MVHOTHER.

Smith, R.B., 1982. ALPEX update. Bull. Am. Meteor. Soc. 63 (2), 186–188. https://doi.org/10.1175/1520-0477-63.2.186.

Tiesi, A., Mazzà, S., Conte, D., Ricchi, A., Baldini, L., Montopoli, M., Picciotti, E., Vulpiani, G., Ferretti, R., Miglietta, M.M., 2022. Numerical simulation of a Giant-Hail-bearing Mediterranean supercell in the Adriatic Sea. Atmosphere 13 (8), 1219. https://doi.org/10.3390/ATMOS13081219.